Invited research Article

The spatio-temporal structure of the Lateglacial to early Holocene transition reconstructed from the pollen record of Lake Suigetsu and its precise correlation with other key global archives: Implications for palaeoclimatology and archaeology

Takeshi Nakagawa [a,b,*], Pavel Tarasov [c], Richard Staff [d,e], Christopher Bronk Ramsey [d], Michael Marshall [f,g], Gordon Schlolaut [h], Charlotte Bryant [e], Achim Brauer [h], Henry Lamb [f,i], Tsuyoshi Haraguchi [j], Katsuya Gotanda [k], Ikuko Kitaba [a], Hiroyuki Kitagawa [l], Johannes van der Plicht [m], Hitoshi Yonenobu [n], Takayuki Omori [o], Yusuke Yokoyama [p], Ryuji Tada [q], Yoshinori Yasuda [r], Suigetsu 2006 Project Members [1]

[a] Research Centre for Palaeoclimatology, Ritsumeikan University, Shiga 525-8577, Japan
[b] Department of Geography, University of Newcastle, Newcastle upon Tyne NE1 7RU, UK
[c] Institute of Geological Sciences, Paleontology, Freie Universität Berlin, Berlin 12249, Germany
[d] Research Laboratory for Archaeology and the History of Art, University of Oxford, Oxford OX1 3TG, UK
[e] Scottish Universities Environmental Research Centre, University of Glasgow, East Kilbride G75 0QF, UK
[f] Department of Geography and Earth Sciences, Aberystwyth University, Aberystwyth SY23 3DB, UK
[g] Institute of Education, University of Derby, Derby DE22 1GB, UK
[h] German Research Centre for Geosciences (GFZ), Section: Climate Dynamics and Landscape Evolution, Telegrafenberg, Potsdam 14473, Germany
[i] Botany Department, School of Natural Sciences, Trinity College Dublin, Dublin 2, Ireland
[j] Department of Biology and Geosciences, Osaka City University, Osaka 558-8585, Japan
[k] Faculty of Global Studies, Chiba University of Commerce, Chiba 272-8512, Japan
[l] Institute for Space-Earth Environmental Research, Nagoya University, Nagoya 464-8601, Japan
[m] Department of Isotope Research, Energy and Sustainability Research Institute, University of Groningen, Groningen, 9747, AG, the Netherlands
[n] College of Education, Naruto University of Education, Naruto 772-8502, Japan
[o] The University Museum, The University of Tokyo, Tokyo 113-0033, Japan
[p] Atmosphere and Ocean Research Institute, Department of Earth and Planetary Sciences, The University of Tokyo, Chiba 277-8564, Japan
[q] Department of Earth and Planetary Sciences, Faculty of Science, The University of Tokyo, Tokyo 113-0033, Japan.
[r] Museum of Natural and Environmental History, Shizuoka, Shizuoka 422-8017, Japan

ARTICLE INFO

ABSTRACT

Leads, lags, or synchronies in climatic events among different regions are key to understanding mechanisms of climate change, as they provide insights into the causal linkages among components of the climate system. The well-studied transition from the Lateglacial to early Holocene (*ca.* 16–10 ka) contains several abrupt climatic shifts, making this period ideal for assessing the spatio-temporal structure of climate change. However, comparisons of timings of past climatic events among regions often remain hypothetical because site-specific age scales are not necessarily synchronised to each other. Here we present new pollen data ($n = 510$) and mean annual temperature reconstruction from the annually laminated sediments of Lake Suigetsu, Japan. Suigetsu's ^{14}C dataset is an integral component of the IntCal20 radiocarbon calibration model, in which the absolute age scale is established to the highest standard. Its exceptionally high-precision chronology, along with recent advances in cosmogenic isotope studies of ice cores, enables temporally coherent comparisons among Suigetsu, Greenland, and other key proxy records across regions.

We show that the onsets of the Lateglacial cold reversal (equivalent to GS-1/Younger Dryas) and the Holocene were synchronous between East Asia and the North Atlantic, whereas the Lateglacial interstadial (equivalent to

GI-1/Bølling-Allerød) started *ca.* two centuries earlier in East Asia than in the North Atlantic. Bimodal migration (or 'jump') of the westerly jet between north and south of the Tibetan plateau and Himalayas may have operated as a threshold system responsible for the abruptness of the change in East and South (and possibly also West) Asia. That threshold in Asia and another major threshold in the North Atlantic, associated with switching on/off of the Atlantic meridional overturning circulation (AMOC), were crossed at different times, producing a multi-centennial asynchrony of abrupt changes, as well as a disparity of climatic modes among regions during the transitional phases. Such disparity may have disturbed zonal circulation and generated unstable climate during transitions. The intervening periods with stable climate, on the other hand, coincided with the beginnings of sedentary life and agriculture, implying that these new lifestyles and technologies were not rational unless climate was stable and thus, to a certain extent, predictable.

1. Definitions

This paper refers to the ages defined by different methods, and synchroneities among them cannot be assumed (Brauer et al., 2014). Therefore, we use the following age units to make the differences clear and to avoid confusion.

IntCal13 yr BP: The absolute age scale assigned to the IntCal13 radiocarbon calibration model (Reimer et al., 2013). The datum (= year 0) is defined at 1950 CE.

IntCal20 yr BP: The absolute age scale assigned to the IntCal20 radiocarbon calibration model (Reimer et al., 2020). The datum is defined at 1950 CE.

GICC05 yr b1.95k: The absolute age scale assigned to the Greenland ice cores (Andersen et al., 2006; Rasmussen et al., 2006; Svensson et al., 2006; Vinther et al., 2006). The original literature uses 2000 CE as the datum and 'b2k' as the unit. In this paper, however, we use 1950 CE as the datum to facilitate comparisons, and indicate the difference by the 'b1.95k' notation. We do not use 'b2k' or any other units that have 2000 CE as the datum, anywhere in this paper.

$SG06_{2012}$ yr BP: Interim age scale assigned to the SG06 sediment core (Bronk Ramsey et al., 2012; Nakagawa et al., 2012) which was used mainly before integration of Suigetsu's dataset into the IntCal calibration models. The datum is defined at 1950 CE.

yr BP: Conceptual 'true' calendar age. The datum is defined at 1950 CE.

U/Th yr BP: Absolute age determined by the Uranium-Thorium method. The datum is defined at 1950 CE.

2. Introduction

2.1. Difficulties of reliable correlation among regions

Leads and lags among regions, or 'spatio-temporal structure' in other words, can hold the key to understanding the mechanisms of climate change. A change that started later in one place cannot be the cause of another change that started earlier in another place. It is important to examine climatic leads and lags at centennial to decadal chronological resolution in order to better understand causal links in the climate system and, if possible, eventually improve climate predictions. The period from the Lateglacial to the early Holocene has particularly attracted research attention as it contains several 'abrupt' climatic transitions with large amplitudes (Clark et al., 2002; Alley et al., 2003), and because it is a relatively recent period in Earth history with better preservation of evidence, denser correlation points, and higher chronological precision than earlier intervals (Björck et al., 1998; Lowe et al., 2001, 2008; Rasmussen et al., 2014). Indeed, there are some pioneering works supported by precise correlation using tephra layers that have successfully reconstructed time-transgressive climate change during the Lateglacial (Lane et al., 2013; Rach et al., 2014).

In the vast majority of cases, however, inter-regional comparison of the timings of these changes is difficult to perform. The Greenland ice cores are synchronised with each other and have a very precise chronology ("GICC05") based principally on counting of ice layers (Andersen et al., 2006; Rasmussen et al., 2006; Svensson et al., 2006; Vinther et al.,

2006). They are well established as the most widely used 'template' of climatic change for the last glacial-interglacial cycle. However, correlations between ice cores and other archives of Late Quaternary environmental change are often problematic because the ice cores contain very little organic matter, and hence do not have a corresponding ^{14}C stratigraphy. Correlation with the ice cores, therefore, needs to rely either on the hypothesis that the different age scales are *per se* coherent with each other (*e.g.* Wang et al., 2001; Nakagawa et al., 2003), or on the tuning of the climate signals (*e.g.* Behl and Kennett, 1996; Hughen et al., 1996). The former, however, carries the risk of mistaking the incoherence of the age scales as a climatic lead or lag signal. The latter, tuning, assumes synchrony of climate changes between regions and thus makes it impossible to discuss any leads or lags (otherwise it would invite circular argument).

Radiometric age determination methods such as radiocarbon (^{14}C) dating do not always ensure reliable correlation either. Marine sediments are normally subject to marine 'reservoir' effects. Traditionally, the marine reservoir effects used to be corrected by assuming that the effect was constant through geological time (*e.g.* Hughen et al., 1996). However, this assumption does not have supporting evidence, and was inevitably the source of multi-centennial uncertainty for robust age-based correlations with marine core records.

Speleothem records are dated by the U/Th method, which provides relatively high chronological precision and accuracy (*e.g.* Wang et al., 2001, 2008; Hoffmann et al., 2010; Southon et al., 2012). The correlation between speleothems and other records often relies on the assumption that calibrated ^{14}C ages are consistent with the U/Th age scale of the speleothems. In theory, other ^{14}C records could be compared with the ^{14}C of the speleothems. However, the radiocarbon dates of the speleothems are subject to a 'dead carbon fraction' (DCF) correction of several centuries or even millennia (*e.g.* Southon et al., 2012; Hoffmann et al., 2010). Speleothems usually do not contain tephra layers, which could otherwise be useful as providing reliable isochrons for correlations.

The uncertainties affect not only correlation but also absolute ages. Ice cores, as well as some annually laminated (varved) sediments, are provided with absolute ages determined by counting of annual layers (*e.g.* Goslar et al., 1995; Hughen et al., 1996; Kitagawa and van der Plicht, 1998a; Zolitschka, 1998; Brauer et al., 2014). However, layer counting inevitably produces a cumulative error (Rasmussen et al., 2006; Bronk Ramsey et al., 2012; Schlolaut et al., 2012; Schlolaut et al., 2018; Adolphi et al., 2018). For example, the GICC05 chronology has a maximum counting error of ± 84 years at 10,000 GICC05 yr b1.95k, which makes it difficult to diagnose centennial-scale lead-lag relationships between Greenland and other regions.

The varved sediments of Lake Suigetsu, central Japan, are in a particularly advantageous position in this global exercise of inter-regional correlation. The numerous ($n > 800$) ^{14}C dates from Lake Suigetsu sediment cores are exclusively on terrestrial plant macrofossils (mostly leaves, but also some bark and twigs), and hence do not require any reservoir or DCF corrections (Kitagawa and van der Plicht, 1998a; Bronk Ramsey et al., 2012). Because Suigetsu's ^{14}C dataset has been adopted as a major part of the IntCal radiocarbon calibration models since 2013 (Reimer et al., 2013, 2020), any terrestrial ^{14}C dates

calibrated using IntCal can be directly correlated with Suigetsu without further corrections. IntCal13 still had a problem with its older part (>32 IntCal13 kyr BP) as it more heavily relied upon Bahamas speleothem data with a relatively large DCF, and therefore the calibrated ^{14}C ages were not tightly tuned to the U/Th timescale. However, the newly released IntCal20 curve uses speleothem data from Hulu Cave, China, which have a much smaller and more constant DCF to the radiocarbon limit, and so the U/Th yr BP and IntCal20 yr BP chronologies have become compatible with each other.

Along with its high-precision and highly correlatable chronology, Suigetsu's varved sediments are also rich in indicators of past climate, including fossil pollen grains. The methods of quantitative climate reconstruction using pollen data are well established for Japan (*e.g.* Nakagawa et al., 2002; Tarasov et al., 2011), so together with the varved nature of the sediment, the Suigetsu cores have the potential to resolve vegetation and climate changes at decadal scale. The unique combination of these features makes Suigetsu an ideal comparison target for assessing spatio-temporal structures of past climate transitions.

Correlation between the Greenland ice cores and archives in other regions has also much improved during the last two decades. The Greenland ice cores, which previously had independent age scales, have been tightly correlated with each other and placed on the common GICC05 chronology (Rasmussen et al., 2014). Blunier et al. (1998) and Blunier and Brook (2001) used ^{10}Be and methane wiggles to synchronise Greenland and Antarctic ice cores, and convincingly showed that the millennial scale climate oscillations during the last glacial period were offset between the respective polar regions, typically with an Antarctica lead. They also proved that the tuning of climate signals is suboptimal as a method to synchronise archives between distant regions. More recently, Svensson et al. (2020) successfully synchronised Greenland and Antarctic ice cores using volcanic signals constrained by layer counts, and established the spatio-temporal structure of the bipolar climatic change at sub-centennial precision.

Muscheler et al. (2014) analysed ^{10}Be wiggles in the GISP2 ice core with the ^{14}C signals in absolutely dated tree ring records, establishing some tie points between GICC05 and tree ring chronologies. They thus demonstrated that the GICC05 timescale is about 65 years too old at the onset of the Holocene, which reverses to an undercount further back into the Lateglacial period. This considerably increased the potential for analysing leads and lags of deglacial climate changes between Greenland and elsewhere at sub-centennial resolution.

Adolphi et al. (2018) applied a similar approach to speleothems. They compared ^{14}C in speleothems and ^{10}Be in GISP2, establishing robust correlations between the GICC05 and U/Th chronologies in the 10–14, 18–25 and 39–45 U/Th kyr BP windows. They then constructed a semi-continuous transfer function with quantified uncertainties by Monte-Carlo simulation taking into account the maximum counting error associated with the GICC05 chronology (Rasmussen et al., 2006). Since the absolute age scale of IntCal20 beyond the 13,910 IntCal20 yr BP tree ring limit is essentially determined by the U/Th chronology of the Hulu speleothem (Reimer et al., 2020), this provided a major breakthrough that enables robust age-based correlation among IntCal, U/Th and ice core chronologies.

The Cariaco Basin also provides one of the most popular comparison targets for Late Quaternary palaeoenvironmental datasets, due to its densely defined ^{14}C stratigraphy and high-resolution palaeoclimate proxy data (*e.g.* Hughen et al., 1996, 1998, 2000, 2004, 2006; Peterson et al., 2000). The Cariaco chronology, however, relied on the assumption of constant marine reservoir age as well as the tuning of the climate signals to Greenland and then Hulu, hindering robust assessment of centennial leads and lags (Hughen et al., 2004, 2006). Recently, however, dynamics of the reservoir effect have been accounted for using Bayesian spline modelling (Hughen and Heaton, 2020), which allowed the Cariaco chronology to be placed on to the IntCal20 timescale. This significantly reduced the uncertainties included in the age-based correlation between Cariaco and U/Th timescales.

In summary, global archives of past climatic changes were poorly correlated with each other some quarter of a century ago. All that we could do was either to believe that different timescales were compatible with each other, or to rely on climate tuning. The INTIMATE network (INTegration of Ice-core, Marine and Terrestrial records; https://intimate.nbi.ku.dk) was launched in 1995 specifically to tackle this problem (Björck et al., 1998). Many of the significant achievements outlined above were generated within the framework of the INTIMATE initiative (Björck et al., 1998; Lowe et al., 2001, 2008; Rasmussen et al., 2014). Today, a quarter of a century after the launch of the group, the synchronisation among ^{14}C, U/Th and ice core chronologies has finally reached the point where assessment of leads and lags at centennial to multi-decadal precision is possible and meaningful (Fig. 1).

### 2.2. Problems with the previous pollen data from Lake Suigetsu

Palaeoclimatological studies using the Suigetsu varves have a 20-year history. Nakagawa et al. (2003, 2005) performed pollen analysis and pollen-based quantitative climate reconstruction using a sediment core recovered in 1993 ('SG93' core). Based on the results, they proposed that: (i) the onset of the Lateglacial interstadial in Japan occurred 300–500 years earlier than in the North Atlantic, (ii) the onset of the Lateglacial cold reversal (known as the Younger Dryas in Europe) was later in Japan than in the North Atlantic region by 250–400 years, and (iii) the onset of the Holocene was later in Japan than in the N. Atlantic by 250 years. Those 'findings' might have had much significance for understanding the mechanisms of the millennial scale oscillations of climate, as well as the threshold systems between orbital forcing and climatic responses, if they were indeed the case. However, these authors' approaches had some critical shortcomings, as follows:

First, the age scale that they relied on was not as accurate as it could have been. The SG93 core had been recovered from a single borehole and had inevitable gaps between sections (Staff et al., 2010). In addition, the absolute age scale of the SG93 core was based on layer counting with the naked eye (Kitagawa and van der Plicht, 1998a, 1998b, 2000). These contributed towards a cumulative counting error of about 6% that was about twice as large as had been previously supposed (Staff et al., 2010). This means that the 'findings' proposed by Nakagawa et al. (2003, 2005) did not have a sound enough chronological basis to robustly assess climatic leads or lags with other regions.

Because of these problems with the SG93 core, the numerous (>300) terrestrial ^{14}C dates obtained from the core were not included in the IntCal98, 04 and 09 radiocarbon calibration models (Stuiver et al., 1998; van der Plicht et al., 2004; Reimer et al., 2004, 2009). Therefore, even terrestrial ^{14}C dates calibrated by the IntCal models could not be directly synchronised with the SG93 core.

The previous pollen data also had problems. The SG93 cores were sliced into 1 cm thick 'disks' through sub-sampling processes. However, because it was not possible to slice cores always at the same seasonal boundary (such as the boundary between the winter and spring pollination seasons), the 'last seasonal layer' to be included in each sub-sample relied entirely on chance. In other words, although the sample thickness was (quasi-) constantly 1 cm, the number of seasonal layers in one sample had ±1 year uncertainty according to the seasons.

The typical sedimentation rate of Lake Suigetsu in the early Holocene was about 1 mm/yr. The 'disk' sub-sample of the SG93 core with 1 cm thickness therefore contained about 10 years. If one such sample contained 10 spring layers and 9 autumn layers, then the result of pollen analysis would have an enhanced spring signal by about 11%, which would clearly represent an artefact of the sampling. Because of this problem, the pollen data contained inevitable noise. Worse still, the higher the chronological resolution that the authors intended to achieve, the larger the signal-to-noise ratio caused by such a mechanism would inevitably become (Nakagawa et al., 2003, 2005).
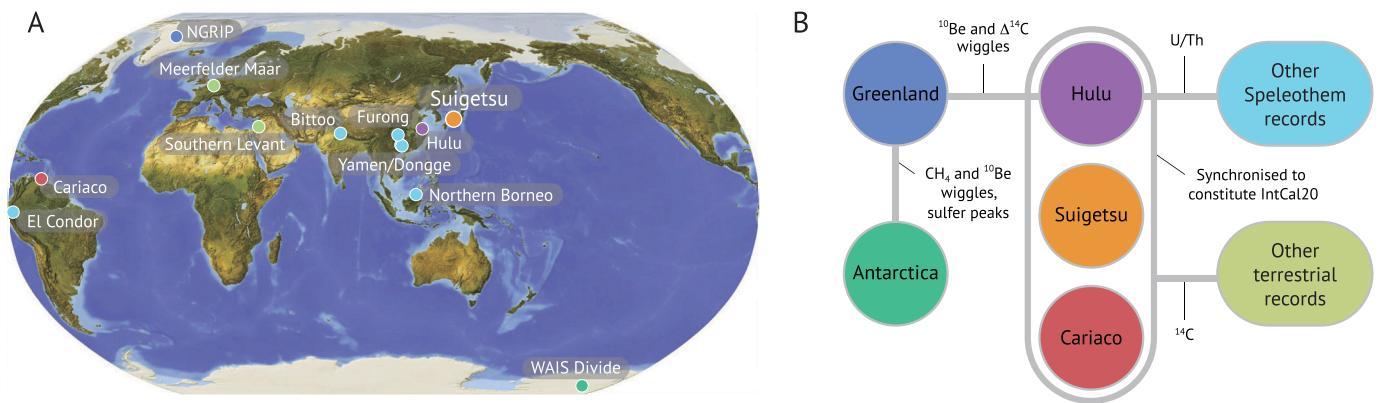
Fig. 1. A: Distribution map of the key sites that constitute the robust correlation network mentioned in the main text. B: Schematic representation showing how key global archives are synchronised with each other.

2.3. Context of this study and palaeoclimatological significance

To remedy the problems outlined above, we started from scratch, with lessons learnt from the previous project. In 2006, we re-drilled the lake to obtain a set of new cores ('SG06') which was used for this study. SG06 consists of sections from 4 parallel boreholes which were drilled within a circle of 20 m radius. The parallel sections perfectly overlap with each other, without any stratigraphic gaps through the whole 73 m sequence (representing the last *ca.* 150 kyr). Fine laminations are present through the upper 45 m (*ca.* 70 kyr) (Nakagawa et al., 2012; Schlolaut et al., 2012, 2018). A ^{14}C dating programme was undertaken, producing 565 new ^{14}C measurements of reservoir-free, terrestrial plant macrofossils from across the entire *ca.* 55,000 year range of the ^{14}C dating method (Staff et al., 2011; Bronk Ramsey et al., 2012). The absolute age scale of the SG06 core was also established by layer counting through a combination of methods (Schlolaut et al., 2012; Marshall et al., 2012), minimising the cumulative counting error through modelling of Suigetsu's ^{14}C dataset to the speleothem ^{14}C records, whilst maintaining rigid relative age constraints provided by the raw layer counts (Bronk Ramsey et al., 2012). The new SG06 age-depth model was also transferred to the previous SG93 core by precise correlation of laminations (Staff et al., 2013b). With these substantial improvements, ^{14}C dates from the SG93 and SG06 cores were adopted as an integral part of the IntCal13 and IntCal20 radiocarbon calibration models (Reimer et al., 2013, 2020), making the composite Suigetsu sedimentary profile an almost ideal template for comparison with other palaeoenvironmental records. As described in more detail below, we also improved the pollen sub-sampling methodology to circumvent the problem of the 'last seasonal layer' effect that enhances the signal from a particular season.

High-resolution pollen analysis of the whole core is still ongoing. However, analysis of the Lateglacial to early Holocene part of the core (16,665 to 10,206 IntCal20 yr BP) at 1 cm stepping has been completed, yielding a total of 510 pollen spectra. Average analytical resolution is 13 years, which enables us to: (i) reconstruct climatic changes during the Lateglacial to early Holocene transition at time intervals that would have been experienced during the lifetimes of contemporary humans, (ii) assess multi-decadal to centennial spatio-temporal structures of abrupt climatic change, and (iii) test the hypotheses of the leads and lags previously proposed by Nakagawa et al. (2003, 2005).

The transition from the Lateglacial to the early Holocene is characterised primarily by a large-scale climatic warming, but also by oscillations between cold (stadial) and warm (interstadial) phases, as well as by abrupt shifts at the boundaries of these phases. Those shifts are often referred to as the most recent examples of abrupt climatic change, and have been intensively studied to attempt to understand the driving

mechanisms of climatic change, the knowledge about which may feed into climate models that we need for future prediction. Although the overall transition can be understood as a non-linear response to the Milankovich orbital forcing, the mechanism behind that non-linearity has not been fully understood. Many hypotheses, such as switching of the three-dimensional ocean circulation (*e.g.* Broecker, 1998), shifts in the atmospheric circulation pattern (Brauer et al., 2008), and even an asteroid impact (Firestone et al., 2007) have been proposed, but the debate is essentially still ongoing.

One notable viewpoint was proposed by Mangerud et al. (2010). Fig. 2 shows a comparison of two segments from the NGRIP δ^{18}O record. Each segment contains two abrupt warming episodes, representing: a) the Lateglacial to early Holocene transition, and b) Dansgaard–Oeschger (D–O) events 7 and 8. The overall similarity of the segments is remarkable. One notable difference, however, is on the right of the figure where the Holocene temperature continues to rise, whereas D–O 7 is short-lived and the glacial condition swiftly resumes (which is typical of D–O events). Although Mangerud et al. (2010) did not argue it explicitly, this alignment exercise gives rise to the following three questions:

1) Was the Lateglacial interstadial of the same nature as other D–O events?
2) Was the Holocene onset triggered by the same mechanism as the D–O events?
3) Can the Holocene be understood as an extended D–O event?

Deglaciation is most likely driven by boreal high-latitudinal summer insolation (Raymo, 1997; Cheng et al., 2009), and the Holocene onset is an integral part of it. However, many pieces of evidence suggest that the Holocene onset was abrupt (*e.g.* Steffensen et al., 2008; Walker et al., 2009), which cannot be explained solely by the (essentially sinusoidal) Milankovich forcing. On the other hand, D–O events are likely driven by switching and hysteresis of the thermohaline circulation (Ganopolski and Rahmstorf, 2001), and the timescale involved is much shorter than that of orbital forcing. It thus seems possible that the Holocene started as the last D–O event, but did not terminate because of the different boundary conditions associated with the Milankovich cycle.

This explanation can be tested by assessing spatio-temporal structures of the abrupt warming episodes. The well age-constrained palaeoclimate records from Suigetsu, Greenland and speleothems, along with application of the transfer function of Adolphi et al. (2018) that allows conversion between U/Th and GICC05 age scales, are best suited for this purpose.

There is a commonly shared view that the millennial-scale climate oscillations in East Asia were largely regulated by the North Atlantic
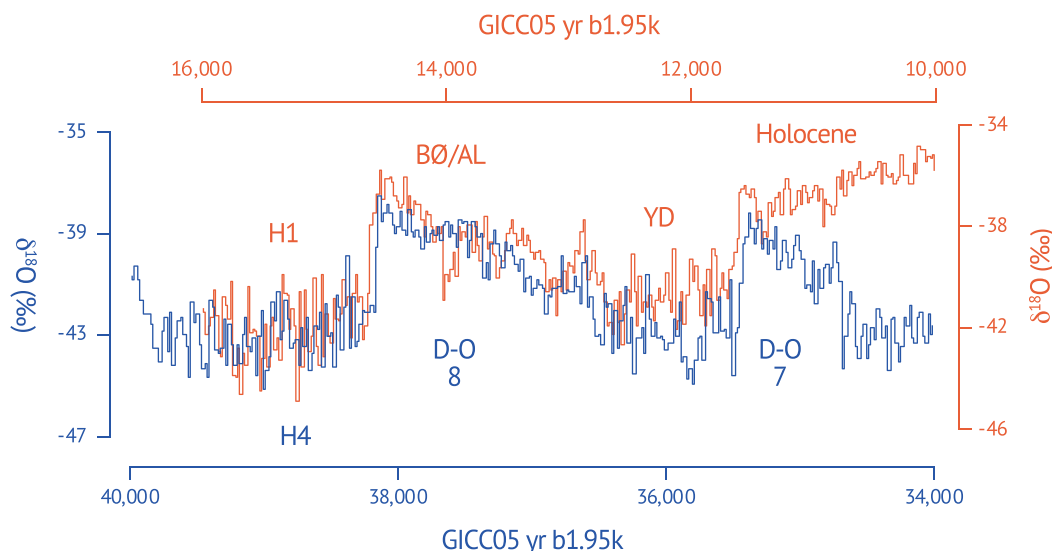
Fig. 2. Two segments from NGRIP δ¹⁸O data (10–16 and 34–40 GICC05 kyr b1.95k) overlain for comparison (modified after Mangerud et al., 2010). These show impressive similarity except where the early Holocene values continue to increase, raising the question as to whether the abrupt warming events that characterise the Lateglacial to early Holocene transition were driven by the same mechanism as D–O events.

processes (namely switching on/off of the AMOC) and that the changes in East Asia and the N. Atlantic are essentially synchronous (Wang et al., 2001; Shen et al., 2010; Corrick et al., 2020). However, most U/Th ages of the speleothems that were used for testing that hypothesis had multi-centennial error ranges, precluding assessment of synchrony/asynchrony with multi-decadal to sub-centennial precision. In this study, we present a microscopic (sub-centennial) yet robust reconstruction of the spatio-temporal structure of the abrupt climate transitions during the
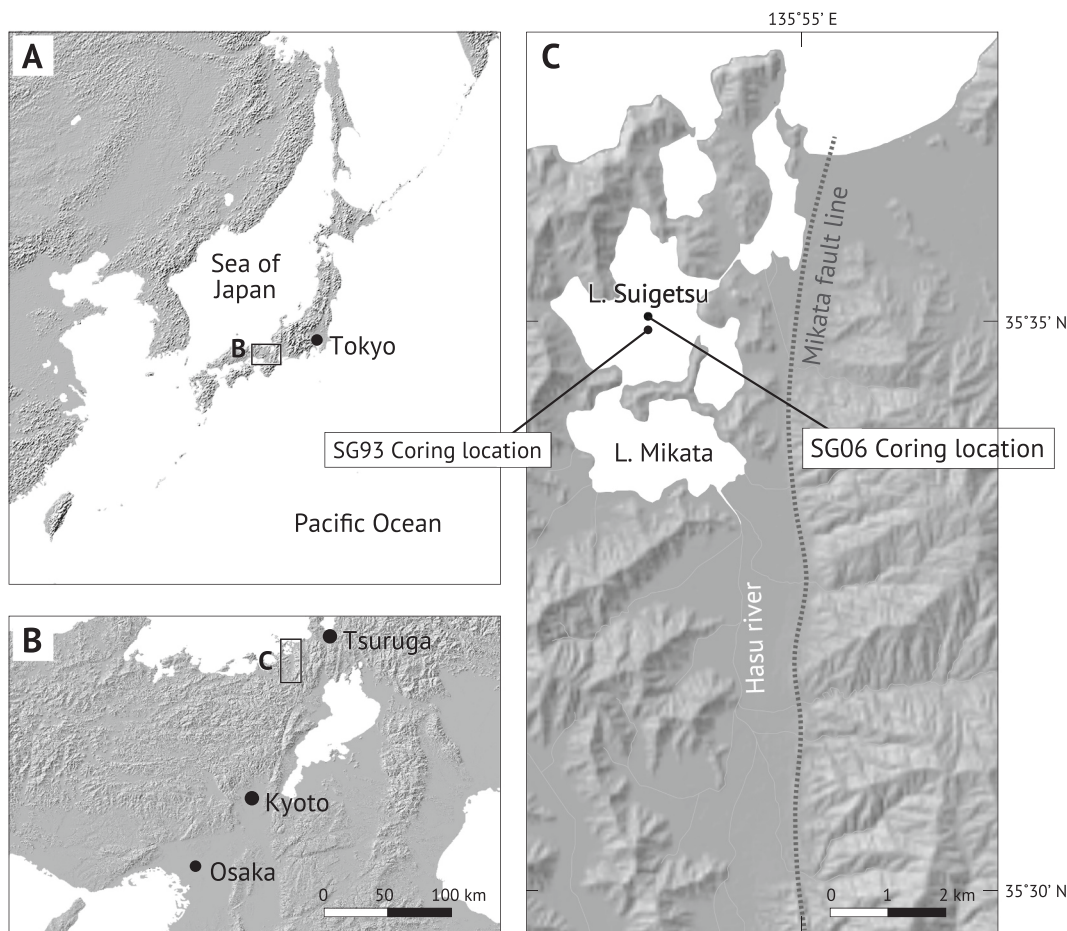
Fig. 3. Location map of Lake Suigetsu, central Japan, and positions of the sediment cores (SG06 and SG93) mentioned in this paper (modified after Nakagawa et al., 2012).

Lateglacial, centring upon new data from Suigetsu and the other best age-controlled archives available to us today, including NGRIP and Hulu.

3. Study site

Lake Suigetsu (35°35′08″ N, 135°52′57″ E) is located close to the Sea of Japan coast of Honshu island, central Japan (Fig. 3). The maximum water depth is 34 m, and the surface area is about 4.2 km². The present elevation is 0 m a.s.l. Diatom analyses of the sediment revealed that it was inundated by sea water during the mid-Holocene and marine isotope stage (MIS) 5e sea level highstands (Saito-Kato, unpublished data). The lake has been brackish since AD1664 through to the present as the lake was then artificially connected to the sea. Otherwise Suigetsu was always a freshwater lake.

Lake Suigetsu is one of the Mikata Five Lakes system, connected to the adjacent lakes through narrow channels. As the lake does not have any inflowing river, the water of Lake Suigetsu is fed exclusively by Lake Mikata and by surface runoff from the surrounding hillsides. Lake Mikata is fed only by the Hasu River, which has a relatively small catchment (27.3 km²) (Fukusawa et al., 1994). Because of this particular setting, Lake Suigetsu is isolated from any high-energy hydrological processes and has an undisturbed, anoxic, and stable lake bottom where varves can accumulate.

The mean annual temperature and the annual precipitation at Tsuruga meteorological observatory, about 18 km to the east of Lake Suigetsu, is 15.3 °C and 2136 mm, respectively (30-year average of AD1981–2010) (Fig. 4). Lake Suigetsu is in the northern margin of the Warm mixed vegetation zone (Cfa climate zone in the Köppen climate classification) (Fig. 5). The nearest Temperate deciduous forest (Dfa climate zone) is on the slope (ca. >600 m a.s.l.) of the surrounding hillsides.

4. Materials and methods

4.1. Sub-sampling varved sediments

The SG06 core is >73 m in length, reaching back to at least MIS-6 at its base (Nakagawa et al., 2012). The upper 45 m are finely laminated, covering the last ca. 70 ka. Details of the SG06 core were already described by Nakagawa et al. (2012), whilst the sub-structure and composition of the annual layers are fully explained by Schlolaut et al.

Fig. 4. Seasonal variability of the temperature and precipitation of Tsuruga city, Fukui prefecture, Japan (30-year average of AD1981–2010).

(2012, 2014, 2018). Sub-samples of the SG06 core for pollen analysis were taken from 1.2 cm-wide LL-channels (https://youtu.be/v5 TEQ8omnr0) (Nakagawa et al., 2012) (Fig. 6) extracted from the composite depth (ver. 06 Apr. 2020) range of 1288.0–1807.7 cm (16,665 ± 36–10,206 ± 14 IntCal20 yr BP). The longitudinal samples taken by LL-channel were sliced mechanically at 1 cm intervals using a "Centi-slicer" device (https://youtu.be/o7TVbzNDT1A). It is important to note that this 1 cm is the interval on the actual LL-channel, i.e. the interval on the idealised composite depth scale is not always precisely 1 cm (the depth of each sub-sample was calculated by dividing the interval between marker layers with defined depths by the number of sub-samples taken from the interval by the Centi-slicer) (Nakagawa et al., 2012; in prep.). The slicing lines were not perpendicular (90°) to the depth axis but were at a 60° angle to the axis in order to avoid the 'last seasonal layer' effect described above (Fig. 7). Theoretically, this should reduce the noise in the seasonal signal from a maximum of 15% down to <2%.

4.2. Pollen analysis and climate reconstruction

In order to determine absolute pollen concentrations, we added 2 ml of "Palynospheres SG06 special blend" marker grain solution (Kitaba and Nakagawa, 2017) to each sample, before any treatments. Palynospheres produced by Palynotech (https://www.palynotech.com) have a density close to that of fossil pollen grains (ca. 1.4 g/cm³), very good visibility under the microscope, and perfect tolerance to any chemical and physical stresses generated during pollen preparation including HF application (though we do not use it routinely) and grinding by sand particles (https://youtu.be/yKqUD32pV6c). The "SG06 special blend" has the grain concentration precisely controlled by the manufacturer, and the grains are dispersed in a non-toxic buoyancy-neutral medium.

The subsamples were then treated by the method of Nakagawa et al. (1998), which has been well established and is summarised as follows:

- 10% HCl (ambient temperature, 8 h)
- 10% KOH (90 °C, 10 min)
- Repeated rinsing (6 times)
- 10% HCl (ambient temperature)
- Heavy liquid separation by $ZnCl_2$ solution (1.88 g/cm³, 2200 r.p.m., 20 min)
- Acetolysis (90 °C, 10 min)
- Ethanol treatment (ambient temperature)
- Mounting in glycerol.

Following the protocol of Nakagawa et al. (2013), we also treated and analysed one standard sample (artificially homogenised Suigetsu sediments) after every 7 real samples. Both pollen and marker grains were identified under light microscopy at 400× magnification and counted using a "PolyCounter" device (https://youtu.be/fs_hgkj0IYE) that enables significantly faster counting. Identification and counting were performed until the total of 32 arboreal taxa identified by Gotanda et al. (2002) as the most representative of the Japanese vegetation reached at least 400 grains. The average number (and the standard deviation) of the 32 arboreal pollen taxa, the total arboreal pollen, and the total arboreal and non-arboreal pollen grains were 436.6 (30.5), 444.1 (32.3), and 476.5 (40.0), respectively. Treatments and analyses were performed in a random order so that any lot-specific bias would not generate a false cyclicity signal. As the pollen signals obtained on the standard samples were generally stable, we did not perform any data correction.

To the percentage data of the 32 pollen taxa, we applied the modern analogue method (Guiot, 1990) that has been well established in Japan (Nakagawa et al., 2002), and reconstructed mean annual temperature. All 32 taxa of Gotanda et al. (2002) were used for reconstruction without enhancing minor taxa. Up to 8 analogues were adopted unless the chord distance exceeded 0.2. Calculations were performed using Polygon 2.4.4 software (http://polsystems.rits-palaeo.com). The surface pollen data
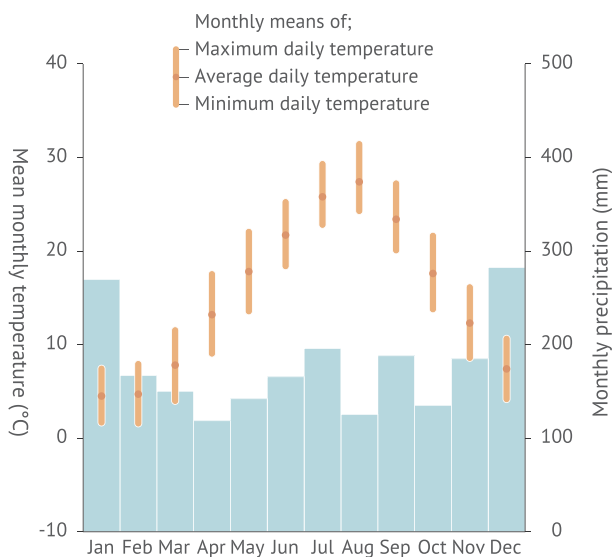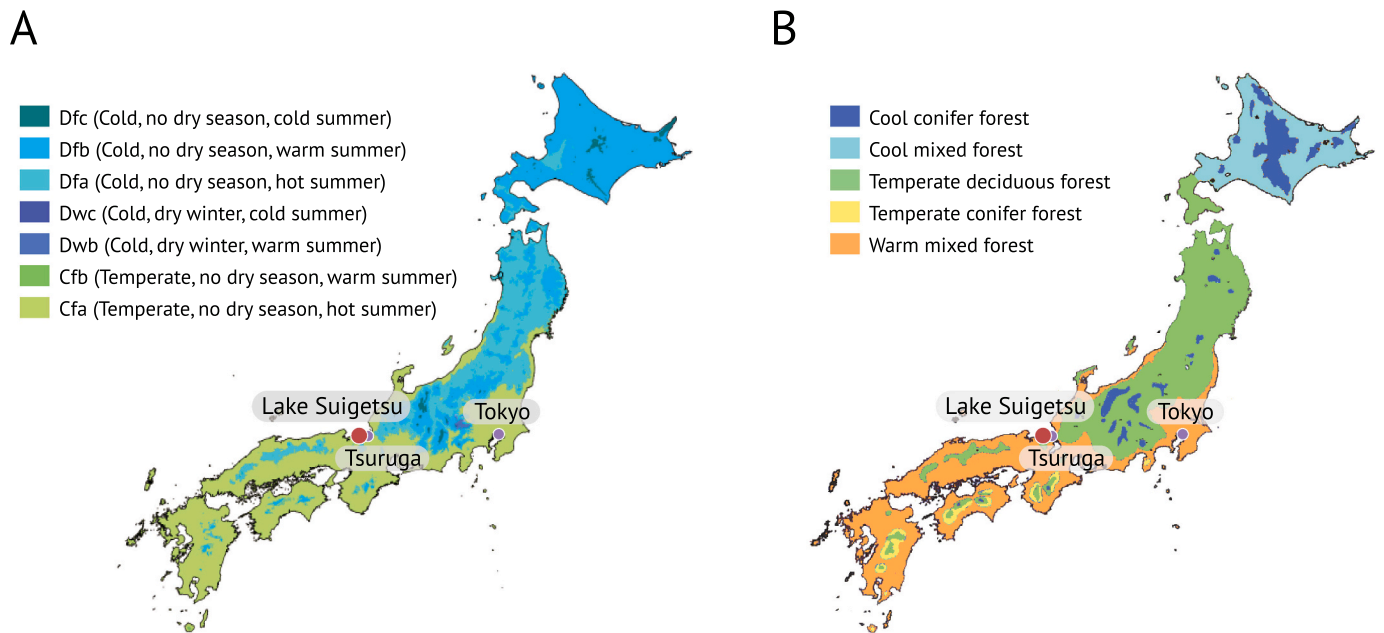
Fig. 5. A: Köppen climate classification of Japan (modified after Beck et al., 2018). B: Potential natural vegetation map of Japan (modified after Yoshioka, 1973). Most of the four main Japanese islands belong to Cfa (Temperate, no dry season, hot summer), Dfa (Cold, no dry season, hot summer), and Dfb (Cold, no dry season, warm summer) zones, which are represented by Warm mixed forest, Temperate deciduous forest, and Cool mixed forest, respectively.

and the modern climate data are also available on the same web site (as of 13 April 2021).

4.3. Updating the age model

Suigetsu's original age scale (SG06$_{2012}$ yr BP chronology) was constructed by wiggle-matching Suigetsu's ^{14}C dataset onto Hulu's (*ca.* 11.2–26.9 U/Th kyr BP) and Bahamas' (*ca.* 28.0–43.9 U/Th kyr BP) speleothem data, with constraints by layer counts and taking into account the possible variation ranges of the DCFs (Bronk Ramsey et al., 2012; Staff et al., 2013a). The older part of the model was, however, not very tightly tuned to the speleothem's U/Th chronology because of the relatively large DCF of the Bahamas speleothem and lack of obvious structures in the Δ^{14}C curve through the *ca.* 30–40 kyr BP period, and was not suitable to put into the transfer function between U/Th and GICC05 chronologies (Adolphi et al., 2018). Subsequently, Suigetsu's ^{14}C dataset was adopted as an integral part of the IntCal13 and IntCal20 radiocarbon calibration models and, thus, the stratigraphy of SG06 is placed directly onto IntCal's absolute chronology. The central archive of IntCal20, from the tree ring limit down to the radiocarbon limit, is that of the Hulu Cave speleothems, which has a significantly smaller DCF than the Bahamas speleothem. This finally makes Suigetsu's IntCal20 yr BP ages suitable for use in the transfer function of Adolphi et al. (2018) for direct comparison with the GICC05 chronology.

In reality, the differences between IntCal13 and IntCal20 chronologies for the period that concerns this study (10.2–16.7 ka) are very small (less than 26 years at the abrupt transitions concerned) and do not affect any conclusions of this paper. Unless otherwise specified, we use IntCal20 yr BP as the default chronology as it is supposed to be the closest to reality, and will facilitate comparison with future terrestrial ^{14}C data that will presumably be calibrated with the latest calibration model.

4.4. Comparison with other sites

Comparison with the Greenland ice cores was performed using the transfer function of Adolphi et al. (2018) assuming Suigetsu's IntCal20 yr BP age to be a sufficiently good surrogate of the U/Th yr BP age used

in that transfer function. Comparison with the Cariaco Basin was made using the IntCal20 yr BP chronology of both sites (Hughen and Heaton, 2020). Comparison with the WAIS Divide ice core relies on the WD2014 chronology and, as with the Greenland ice cores, the transfer function of Adolphi et al. (2018). The WD2014 chronology was established by independent layer counting, but its offset to the GICC05 chronology has been shown to be less than 24 years during the Lateglacial period (which is negligible for the purpose of the present study since the WAIS Divide record does not exhibit as abrupt changes as in Suigetsu and Greenland) (WAIS Divide Project Members, 2013; Sigl et al., 2016). U/Th ages given to the speleothems were directly compared with the IntCal20 ages without conversion because the IntCal20 yr BP chronology beyond the tree ring limit is essentially the U/Th$_{Hulu}$ yr BP chronology.

In order to compare timings of climatic change among regions, we needed to define the start, midpoint and end of the transitions. For this purpose, we performed a ramp function fitting using the EventWatcher program (http://polsystems.rits-palaeo.com). Range-finding was performed with 200,000 initial iterations. Then improved solutions were intensively searched for in the vicinity of the nodes determined by the range finding for at least another 200,000 iterations until the solution did not improve for 100,000 reiterations. We used the same approach for climate curves from Suigetsu and other sites, unless the fitting results were already provided in the original literature (Steffensen et al., 2008).

5. Results and discussion

5.1. Overall trend

Results of the pollen analysis and the quantitative climate reconstruction are shown in Fig. 8. Three visible gaps in the diagram are turbidite layers that do not constitute any significant time gaps (the SG06 core was recovered from the lake's quasi-flat depocentre with minimal erosion potential, as supported by thin section microscopy which did not identify any evidence of removal of materials by those turbidites, and ^{14}C dates which do not exhibit visible jumps at those event layers). Fig. 9A is the reconstructed climate plotted on the age scale. Fig. 9B is the standard deviation of the reconstructed mean annual temperature for a 100 year-long moving window (which contains 7.9
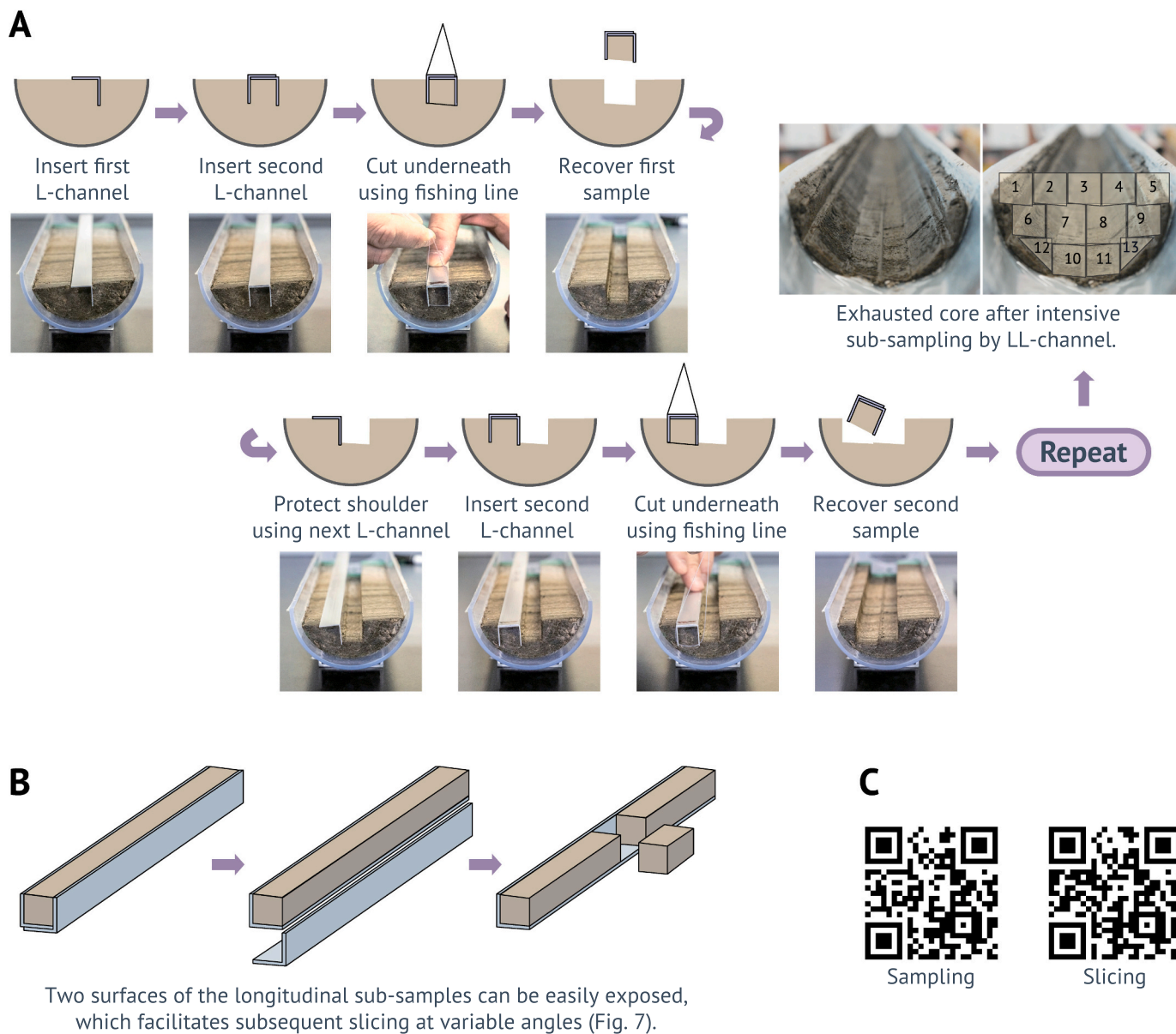
Fig. 6. A: Longitudinal sub-sampling by double-L (LL) channel (modified after Nakagawa et al., 2012). B: Samples taken by LL-channel can be sliced very easily. C: Links to the tutorial videos.

datapoints on average), *i.e.* the larger the value on this diagram, the greater the multi-decadal instability of the climate.

The basal part of the diagram (*ca.* >15.8 kyr BP) (Fig. 8) is characterised by boreal/temperate arboreal species such as *Abies*, *Picea*, *Betula*, and *Quercus* (deciduous type), which are typical of the cool mixed forest that corresponds to the Dfb (Temperate continental/Humid continental) climate zone. The relatively elevated percentage of *Artemisia* indicates that the forest was semi-open. The reconstructed mean annual temperature was about 5 °C, *i.e.* lower than today by about 10 °C. From about 15.8 IntCal20 kyr BP, coniferous trees (such as *Abies* and *Picea*) and *Betula* start decreasing, replaced by broad-leaved trees such as *Alnus*, *Fraxinus*, and *Quercus* (deciduous type). The reconstructed temperature gradually increases with some short-lived 'flickers'. This cold period with some movements towards warmer conditions can be seen as a transition or 'precursor' towards more abrupt warming that occurred *ca.* 15.0 IntCal20 kyr BP. This period is correlated with the local pollen zone SGPS-2 of the old SG93 core described by Nakagawa et al. (2003, 2005).

At *ca.* 14.9 IntCal20 kyr BP, the sudden replacement of *Tsuga* by

Cupressaceae-Taxaceae type pollen, sudden increase of *Fraxinus*, and sharp decrease of *Artemisia* are observed, indicating the replacement of the cool mixed open forest by the temperate deciduous forest. It cannot be denied that such replacement of the vegetation types may have involved some response time. One needs to be cautious, therefore, in detecting lags in the reconstructed climate at this transition. In contrast, if any leads in Suigetsu are observed, then that observation would be robust because the effect of the vegetation response time in the pollen signal must operate in the opposite direction.

After the completion of the vegetation shift at *ca.* 14.7 IntCal20 kyr BP, relatively warm conditions persisted until *ca.* 12.8 IntCal20 kyr BP, with gradually increasing temperature (Fig. 9A) and gradually decreasing variability of temperature (Fig. 9B). Most of the climate oscillations that characterise the lower (earlier) part of this interval (that roughly corresponds to the Bølling period in Europe) are represented by multiple sub-samples, *i.e.* they are not noise in the pollen data but represent real multi-decadal signals (*c.f.* insets A-B of Fig. 8; *N.B.* average analytical interval for this period is 12.7 years). This relatively
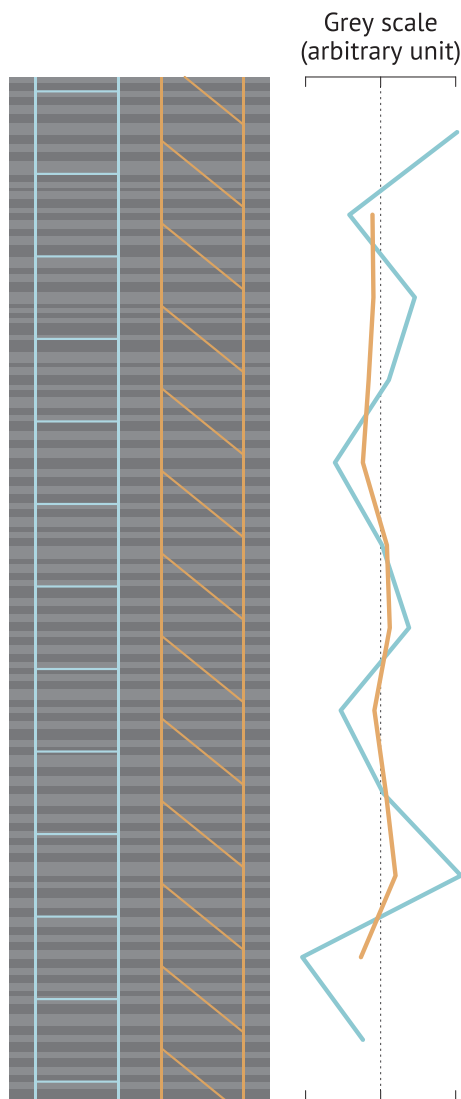
Fig. 7. Diagonal slicing of LL-channel subsamples. Thicknesses of the idealised varves shown here are normally distributed around 1 (arbitrary unit) with a standard deviation of 0.25, without any longer-term trend. Light blue lines denote perpendicular slicing (90° to the axis) at an interval of 10 units. Orange lines denote diagonal slicing at 60° to the axis at an interval of 10 units. Curves in corresponding colours show average grey-scale values of each sub-sample taken by the different slicing strategies. The perpendicular slicing generates a much stronger false signal caused by the 'last seasonal layer' effect.

warm period is correlated with the local pollen zone SGPI-1 previously recognised by Nakagawa et al. (2003, 2005) from the old SG93 core.

Based on the pollen data of the SG93 core, Nakagawa et al. (2003, 2005) divided this zone into subzones a-c. However, we cannot observe such clearly defined phases in the new record. The subzones in the previous studies were most likely artefacts due to suboptimum data quality.

From *ca.* 12.8 to *ca.* 11.6 IntCal20 kyr BP, *Fagus* (*crenata* type) increases, with significantly lower reconstructed temperatures. Throughout this period, both *Fagus* pollen and reconstructed temperature demonstrate unstable multi-decadal oscillations. Most of the oscillations are represented by more than one sample, supporting our interpretation that they are not noise but represent real signals. The instability index (the standard deviation; Fig. 9B) is accordingly very high during this period. This zone is correlated to the local pollen zone SGPS-1 of the SG93 pollen data (Nakagawa et al., 2003, 2005). This relatively cold and unstable period corresponds to the Lateglacial cold

reversal that is often referred to as the 'Younger Dryas' in Europe or 'GS-1' in Greenland (Björck et al., 1998).

Fagus crenata type pollen that characterised the cold reversal period suddenly decreases at *ca.* 11.6 IntCal20 kyr BP, marking the start of the Holocene. Instead, *Castanopsis-Castanea* type pollen starts increasing gradually. The reconstructed temperature rises abruptly at the base of this zone, then the climate stayed relatively warm and stable throughout this period. This warm period is correlated with the local pollen zone SGPH defined on the SG93 core by Nakagawa et al. (2005).

Changes at both the onsets of the Lateglacial cold reversal (at *ca.*12.8 IntCal20 kyr BP) and of the Holocene (at *ca.* 11.6 IntCal20 kyr BP) were not total replacements of vegetation types but were instead relative changes in the abundance and/or vigour of already existing members of the local vegetation. The response time of the pollen signal is, therefore, assumed to have been rapid. The fact that we can resolve decadal-scale oscillations (which would otherwise have been smoothed) also supports the ability of this pollen-based temperature record to detect not only leads but also lags and/or synchrony when compared to other records (insets A-B of Fig. 8).

The sequence of climatic changes outlined above roughly mirrors the climatic episodes reported for the Lateglacial to early Holocene transition in the North Atlantic region, *i.e.* stadial – interstadial – cold reversal – Holocene (GS-2 - GI-1 - GS-1 - Holocene in Greenland, or Heinrich 1 – Bølling/Allerød – Younger Dryas – Holocene in northern Europe) (Fig. 10). However, it does not show a similarity to the tropical Western Pacific (Fig. 10F) or Antarctica (Fig. 10G) where changes were generally more gradual and the cold reversal (when it exists) does not coincide with that of Greenland (Partin et al., 2007; Pedro et al., 2015). In the broadest sense, therefore, Japan "belongs" to the N. Hemispheric regime, which is typically represented by Greenland (and also Hulu Cave, in East Asia). Notable differences with Greenland include a much smaller amplitude of the cold reversal, greater climatic stability during the second half of the interstadial, and the gradual increase of temperature throughout the interstadial.

The cooling trend that persists during the Lateglacial interstadial in Greenland (GI-1) is a shared structure with D–O events (Fig. 2) and thus provides intuitive support for the view that the Lateglacial interstadial is the latest D–O event (D–O 1). On the other hand, the temperature keeps rising during the same period in Suigetsu, China, Borneo, and partly in Antarctica until the Antarctic cold reversal (ACR) starts (Fig. 10D-G), following the N. hemispheric summer insolation change in high-latitudinal regions (Fig. 10I). This supports orthodox views that the deglaciation is largely driven by rising insolation in the N. hemispheric summer (Raymo, 1997; Cheng et al., 2009), with a superimposed influence from the switching on/off of the thermohaline circulation (Broecker, 1998) which exhibits strong bimodality and hysteresis that generates an abrupt and amplified response in the N. Atlantic (Ganopolski and Rahmstorf, 2001). The abrupt warming at the onset of the interstadial in the N. Atlantic was swiftly followed by a gradual return to the stadial mode, with limited influence on other regions such as monsoonal Asia (*e.g.* Wang et al., 2001).

The amplitude of the Lateglacial cold reversal (equivalent to the Younger Dryas) is smaller in Japan than in the N. Atlantic (Schlolaut et al., 2017). Nakagawa et al. (2006) reported that the degree of cooling in Japan was significantly larger in winter when Japan is governed by the Eurasian airmass, whereas it is much smaller in summer when Japan is under the Pacific airmass. These observations can be coherently explained if the Eurasian airmass is more strongly linked to the N. Atlantic, but the N. Atlantic influence is attenuated at the monsoon front (boundary between Eurasian and Pacific airmasses) and hardly reaches the W. Pacific. This interpretation is also in line with the N. Borneo and Antarctic evidence where no Younger Dryas-like oscillation is observed.

5.2. Timings of the climatic changes in detail

The starts, midpoints, and ends of the three transitions recognised by
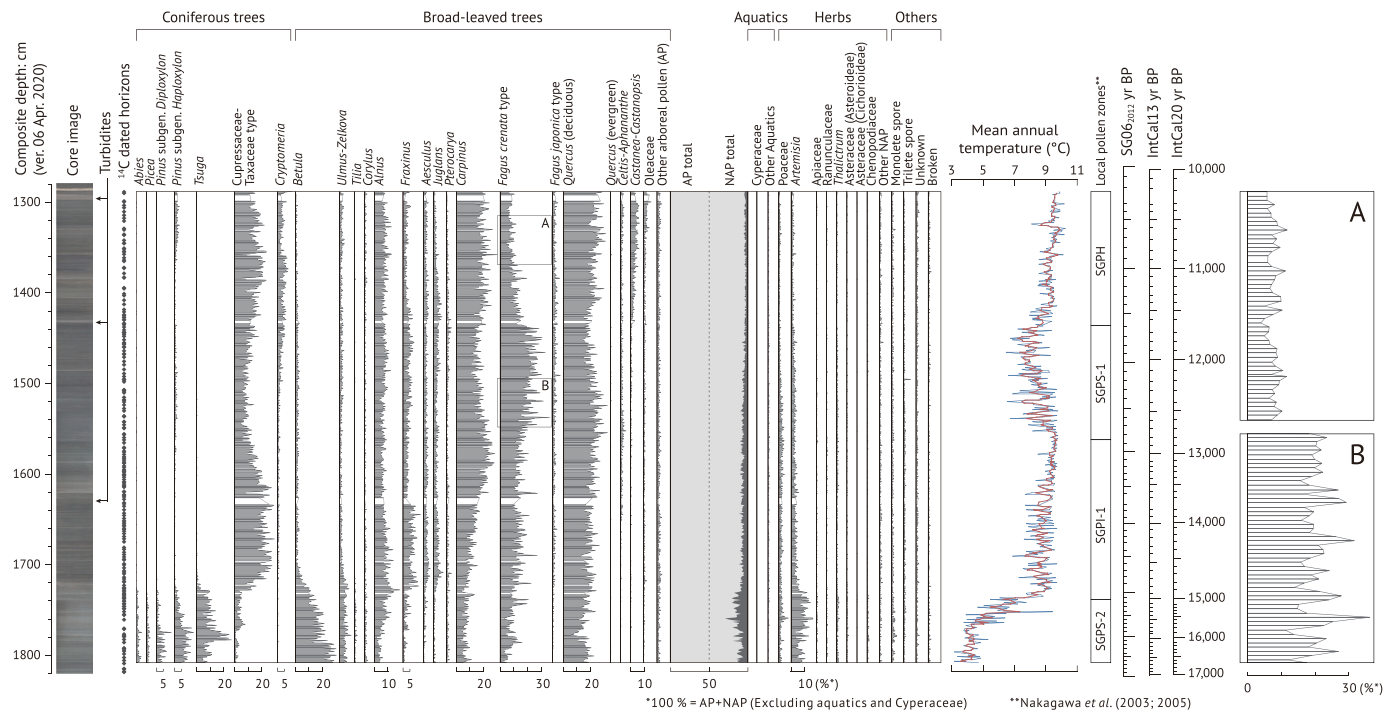
Fig. 8. Full pollen diagram and reconstructed mean annual temperature plotted against composite depth (ver. 06 Apr. 2020) (Nakagawa et al., 2012). AP: arboreal pollen. NAP: non-arboreal pollen. Percentage values were calculated on the basis of the sum of AP and NAP, including *Alnus* and *Salix*, excluding aquatic plants, Cyperaceae, and all other palynomorphs. Local pollen zones were taken after Nakagawa et al. (2003, 2005). Blue line: raw reconstruction. Red line: three point moving average. Insets: close-up views of typically stable (A) and unstable (B) periods of the Holocene and the Lateglacial cold reversal, respectively. Most oscillations during the unstable period are represented by multiple data points.

the ramp function fitting are summarised in Table 1. Also shown in Table 2 are those data for Greenland recognised from the *D*-excess data of the NGRIP ice core (Steffensen et al., 2008). The left-hand side of Fig. 11 (A-C) shows a detailed comparison between both sites for the three climatic transitions from the Lateglacial to the early Holocene. IntCal20 yr BP and GICC05 yr b1.95k age scales in the figure are synchronised using the transfer function of Adolphi et al. (2018).

The right-hand side of Fig. 11 (D–F) shows images of the SG06 varved sediment core around the depth of each transition. The transitions recognised by ramp function fitting both in SG06 and NGRIP cores are also projected on to the core images. The transitions in Suigetsu do not have error bars because they were directly measured on those cores (the only factor to generate uncertainty in the position on the core is the sample size, which is 1 cm in the case of this study). On the other hand, the projection of the transition in NGRIP on to the SG06 core is the combination of age uncertainties associated with both records and the transfer function. The combined uncertainty ranges at 1 and 2 sigma are indicated beside the core images.

Each of the three transitions has a unique spatio-temporal structure. Their details and implications are described below (in reverse chronological order because the observations for the later transitions are used to interpret those for the earlier transition).

5.2.1. Holocene onset

The Holocene onsets in Suigetsu and Greenland were both abrupt, and their timings were synchronous within 1 sigma error (Fig. 11A). In Suigetsu, the fitted ramp function has a duration of 10.2 years. This duration, however, is below the level of significance because the sampling interval (and hence the number of years included in each subsample) around this horizon is about 10 years. On the other hand, the core image shows a clear boundary in the sedimentary facies; the varves below the Holocene onset are thinner and darker in colour, whereas

those above the onset are thicker and lighter (Fig. 11D). The mechanism behind this difference is not fully understood. However, the visible sharp boundary in the annually laminated sediment strongly implies that the sedimentary and/or catchment environments changed from stadial to Holocene modes possibly within a single year. This is also in line with the NGRIP record that indicates that the wind system shifted drastically in a matter of a 'few years' (Steffensen et al., 2008).

When projected on to the SG06 core, the midpoints of the changes in Suigetsu and NGRIP are less than 2 cm (*ca.* 20 years) apart. This is a surprisingly good agreement, taking into account the uncertainties included in the transfer function of Adolphi et al. (2018) as well as the sampling interval in Suigetsu. We consider that the synchroneity of the Holocene onset between Greenland and Suigetsu is therefore robustly supported by this agreement.

The above conclusion negates the asynchrony of the Holocene onset argued by Nakagawa et al. (2003, 2005). The previous conclusions were erroneous because the Suigetsu and GRIP chronologies were not properly synchronised, and the lead author of the papers was not fully aware of the discrepancies among different age scales. (One reviewer of the Nakagawa et al. (2003) paper carefully observed the ^{14}C dataset of Suigetsu and pointed out the likelihood that the conclusion was erroneous (Björck, personal communication)).

At the onset of the Holocene, the temperature at Suigetsu rose by about 2–3 °C. Before the transition, the climate was unstable, and the temperature was oscillating on a multi-decadal timescale by about a few degrees. However, the climate became much more stable after the transition (Fig. 9B).

5.2.2. Onset of the Lateglacial cold reversal

The onset of the Lateglacial cold reversal (also referred to as the Younger Dryas, GS-1 or Heinrich 0 according to the locality and context) was abrupt in the circum N. Atlantic region including in Greenland and
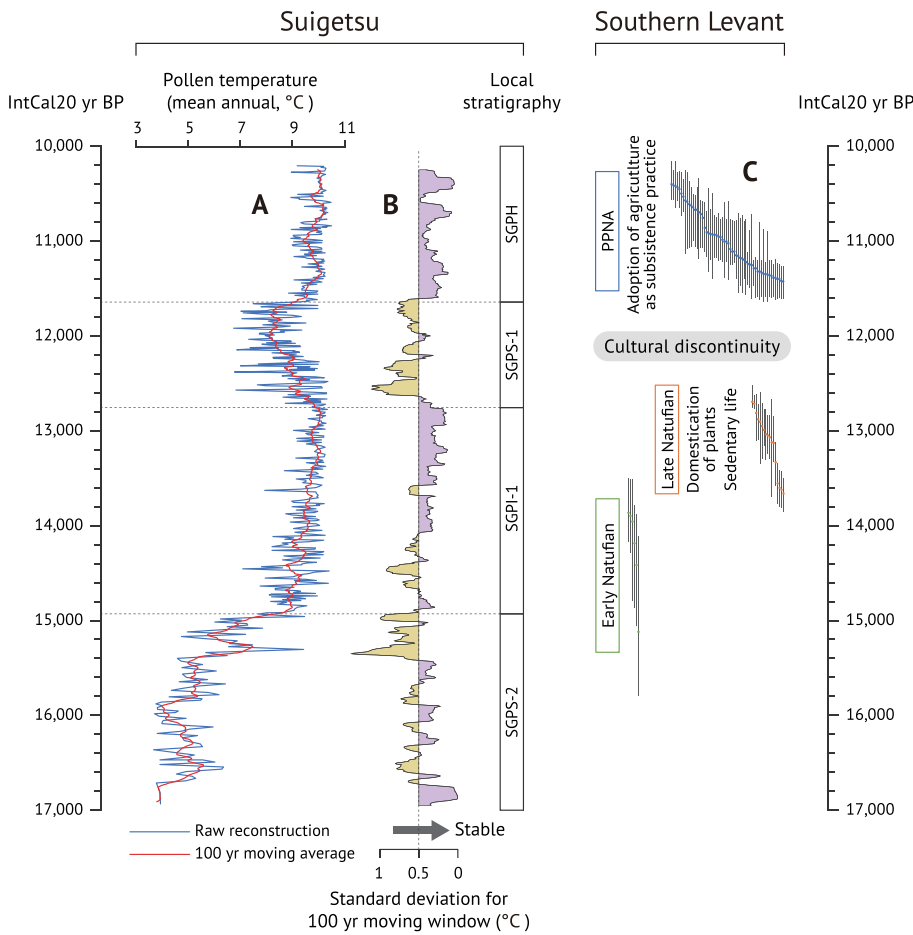
Fig. 9. A: Reconstructed mean annual temperature plotted against IntCal20 age axis. Blue line: raw reconstruction. Red line: 100 year moving average. B: Standard deviation of the reconstructed temperature in 100 year moving window. The horizontal axis is inverted, *i.e.* the purple colour on the right-hand side indicates that the climate was stable during the century. C: Radiocarbon dates of Natufian and Pre-pottery Neolithic-A (PPNA) cultures after screening, calibration and Bayesian modelling (modified after Blockley and Pinhasi, 2011) (re-calculated from raw ¹⁴C dates using IntCal20 for coherence with curves A and B), with archaeological contexts. Both the late Natufian and PPNA cultures coincide with warm and stable periods.

Fig. 10. A-H: Synchronised palaeoclimate reconstructions from across regions. A: Lake Suigetsu pollen-derived temperature. B-C: $\delta^{18}O$ and *D*-excess of the NGRIP ice core (Steffensen et al., 2008). D-E: $\delta^{18}O$ of Hulu and Yamen caves, China (Wang et al., 2001; Yang et al., 2010). F: $\delta^{18}O$ of speleothems from three caves in Northern Borneo (Partin et al., 2007). G: $\delta^{18}O$ of WAIS Divide ice core from Antarctica (WAIS Divide Project Members, 2013). H: 550 nm reflectance from the Cariaco basin (Hughen and Heaton, 2020). I: summer insolation at 35°N, the latitude of Lake Suigetsu (Laskar et al., 2004). Light yellow bands correspond to the three higher resolution intervals shown in Fig. 11. Black dotted lines denote transitions in Suigetsu and NGRIP. Error bands show 1 sigma (black) and 2 sigma (grey) uncertainties.

Table 1

Results of the ramp function fitting to the pollen-based reconstructed mean annual temperature in Suigetsu, for the three climate transitions discussed in this paper.

	IntCal20 yr BP	Age error (±1 sigma)	Age error (±2 sigma)	Mean annual temperature (°C)	Note
Model end	11,400.0	26.4	52.8	9.59	
Ramp end	11,637.9	34.5	68.9	9.59	
Ramp midpoint*	11,643.0	34.2	68.4	8.97	*Onset of the Holocene
Ramp start	11,648.1	33.9	67.8	8.34	
Model start	12,000.0	21.7	43.3	8.34	
Model end	11,700.0	29.0	58.0	8.28	
Ramp end	12,023.0	22.0	44.0	8.28	
Ramp midpoint	12,434.3	20.5	40.9	9.13	
Ramp start**	12,845.5	22.2	44.5	9.98	**Onset of the Lateglacial cold reversal
Model start	13,100.0	19.3	38.6	9.98	
Model end	14,500.0	36.4	72.7	8.95	
Ramp end	14,963.7	41.4	82.8	8.95	
Ramp midpoint***	14,969.8	41.0	82.1	7.67	***Onset of the Lateglacial interstadial
Ramp start	14,975.8	40.8	81.7	6.39	
Model start	15,500.0	42.1	84.3	6.39	

Table 2

Results of the ramp function fitting to the *D*-Excess in NGRIP ice core, for the three climate transitions discussed in this paper (Steffensen et al., 2008).

	GICC05 b1.95k	U/Th yr BP	Age error (−2 sigma)	Age error (−1 sigma)	Age error (+1 sigma)	Age error (+2 sigma)	D-excess (‰)	
Model end	11,500.0	11,465.6	15.6	7.3	5.2	12.5	8.45	
Ramp end	11,651.0	11,624.5	16.0	7.4	6.4	14.9	8.45	
Ramp midpoint*	11,652.5	11,626.1	16.0	7.4	6.4	14.9	9.44	*Onset of the Holocene
Ramp start	11,654.0	11,627.7	16.0	7.4	6.4	14.9	10.44	
Model start	11,800.0	11,781.9	18.4	7.4	8.5	16.0	10.44	
Model end	12,600.0	12,600.0	14.3	7.1	5.0	13.0	9.73	
Ramp end	12,846.0	12,845.9	12.9	5.9	7.1	16.6	9.73	
Ramp midpoint**	12,846.5	12,846.4	12.9	5.9	7.1	16.6	8.57	**Onset of the Lateglacial cold reversal (GS1)
Ramp start	12,847.0	12,846.9	12.9	5.9	7.1	16.6	7.41	
Model start	13,100.0	13,107.6	15.9	8.7	9.8	20.7	7.41	
Model end	14,500.0	14,596.8	95.8	48.8	43.2	91.8	6.16	
Ramp end	14,641.0	14,741.1	100.1	48.2	53.5	104.4	6.16	
Ramp midpoint***	14,642.5	14,742.8	100.3	48.4	53.4	104.4	7.86	***Onset of the Lateglacial interstadial (GI1)
Ramp start	14,644.0	14,744.4	100.4	48.5	53.4	104.5	9.57	
Model start	14,800.0	14,914.4	113.4	57.3	53.0	106.7	9.57	

at Meerfelder Maar, Germany. (Brauer et al., 2008; Steffensen et al., 2008; Bakke et al., 2009). In Suigetsu, by contrast, the onset is more gradual than abrupt, and the fitted ramp function has a duration of >800 years (Fig. 11B; Table 1). The ramp midpoint lags behind that of NGRIP by several hundred years. However, the start of the ramp in Suigetsu is again in surprisingly good agreement with the start of GS-1 in NGRIP. The midpoints of the probability distributions of the ages are less than 1 cm apart from each other as expressed as their equivalent position on the SG06 core, which is well within the error of the transfer function and even of the sampling interval (Fig. 11E).

In conclusion, the onset of the Lateglacial cold reversal exhibits a very high level of synchrony between Greenland and Suigetsu (which also negates Nakagawa et al., 2003, 2005). This new finding does not contradict the widely accepted scenario that the cold reversal was triggered by a meltwater pulse (MWP) from the Laurentide Ice Sheet and caused by the shutting down of the thermohaline circulation (Broecker, 1998; Stocker and Johnsen, 2003; Barker et al., 2009), which was then transmitted to East Asia through an atmospheric teleconnection (Wang et al., 2001).

There is a claim that the onset of the Lateglacial cold reversal was triggered by an asteroid impact (*e.g.* Firestone et al., 2007), which is not necessarily widely accepted, but still attracts a considerable number of researchers (*e.g.* Kennett et al., 2009; Moore et al., 2020). The principal line of 'evidence' to support the claim is the high concentration of iridium in the 'Younger Dryas boundary' layer in lacustrine sediments in many places in North America that mark the beginning of the cold

reversal. Because Lake Suigetsu was a stable sedimentary basin and the annually laminated layers were not subject to vertical mixing, the iridium-rich dust (if it did shower Japan) should be preserved and show a sharp iridium peak in the sediment.

Layer counting of the SG06 core was performed by two different methods (Marshall et al., 2012; Schlolaut et al., 2012), one of which was based on high-resolution scanning by Itrax X-ray fluorescence (XRF) scanner. This used a 100 μm wide flat beam and the analytical stepping was 60 μm, which means that each adjacent pair of measurements overlapped by 40% (Marshall et al., 2012). SG06 consists of parallel sections that also overlap with each other, without allowing any core gaps (Nakagawa et al., 2012). If there were to be an iridium-rich layer, therefore, the XRF data should have picked up the signal.

Fig. 11E shows the curve of the iridium XRF counts overlain on the corresponding SG06 core image. There is no visible peak in iridium across the *ca.* 250-year long period that certainly encompasses the onset of the Younger Dryas. This does not provide conclusive evidence to reject the asteroid impact hypothesis of the Younger Dryas; but it does suggest that the supposed iridium-rich dust shower did not reach Lake Suigetsu. This could be used as a robust boundary condition to estimate the magnitude of the impact, if there was one.

5.2.3. Onset of the Lateglacial interstadial

The onset of the Lateglacial interstadial had a different spatio-temporal structure from the other transitions described above. The onset in Suigetsu was abrupt and led that in Greenland by about two
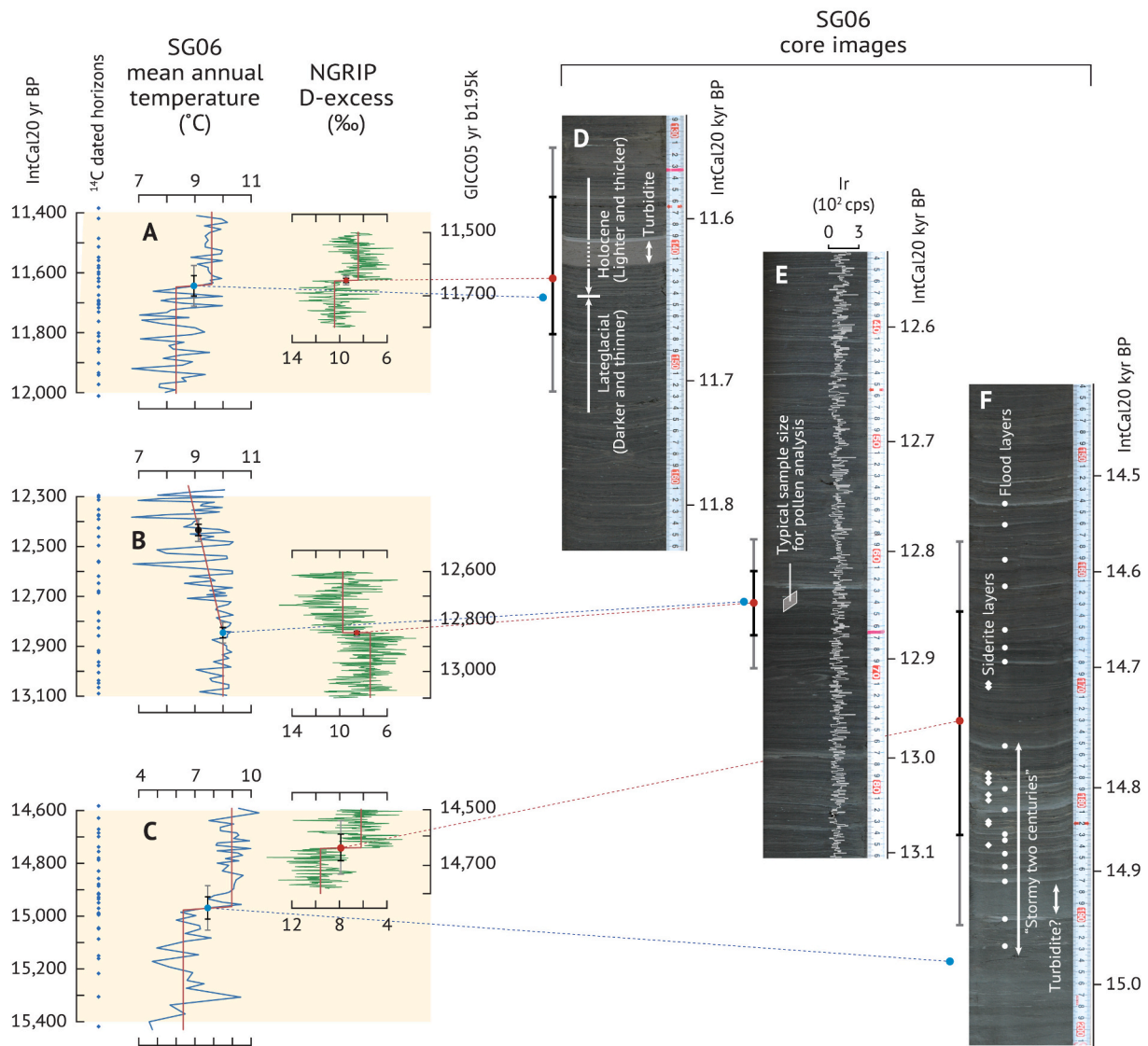
Fig. 11. Detailed comparison of timings between Suigetsu and NGRIP at: the Holocene onset (A), the onset of the Lateglacial cold reversal (B), and the onset of the Lateglacial interstadial (C). Also shown are SG06 sediment core images that correspond to the three transitions (D–F). Transitions recognised by ramp function fittings (red lines) are indicated both on the data and core images by circles in corresponding colours. Error bands are shown at 1 sigma (black) and 2 sigma (grey) uncertainties. *N.B.* data and core images are presented on different age axes.

centuries. The offset was beyond 2 sigma errors (Fig. 11C). The age difference between ramp midpoints in Suigetsu and NGRIP was 227.0 + 94.4/−89.4 IntCal20 years at 68.3% confidence interval (equivalent to 1 sigma), and 227.0 + 186.5/−182.4 IntCal20 years at 95.4% confidence interval (equivalent to 2 sigma). Because the temperature change in Japan leads that of Greenland (a conclusion that would not be invalid even if the pollen-inferred temperature increase involved a lagged vegetation response to climate), we can conclude that the onset of the Lateglacial interstadial was indeed asynchronous between Japan and Greenland. This conclusion affirms the asynchrony claimed by Naka-gawa et al. (2003, 2005).

The sedimentary facies also show interesting features across this transition (Fig. 11F). Immediately after the abrupt warming in Suigetsu, the frequency of characteristic light grey layers increases. According to the comparison between sedimentary facies in Suigetsu and the instru-mentally measured climate of the last *ca.* 90 years, such clay layers are typically deposited after major flooding events (mostly caused by ty-phoons) (Suzuki et al., 2016). Also particularly abundant during this period are light yellowish siderite layers. The mechanisms for siderite layer formation in Suigetsu have not been fully understood, but

represent an 'unusual' (infrequent) situation over the longer term, of which one candidate cause could be enhanced input of iron-rich soil from the catchment area (Schlolaut et al., 2014) due to forest destruction by landslides (which in turn were caused by waterlogging of surface soil) and/or strong winds. The frequent deposition of clay and siderite layers, therefore, implies that the Lake Suigetsu region was stormy during this period of transition.

After the earlier interstadial onset in East Asia/the West Pacific than in the North Atlantic, there existed a transitional period during which the longitudinal temperature balance across Eurasia was disturbed. This could have made the zonal circulation over Eurasia unstable, resulting in the 'stormy two centuries' in Suigetsu. This unstable condition could have been common across Eurasia, as is suggested by the increased deposition of detrital layers in Meerfelder Maar prior to the onset of the Lateglacial interstadial (Brauer, unpublished data). About 230 years later, the thermohaline circulation resumed and the circum-N. Atlantic regions became warmer, which re-established the longitudinal temper-ature balance over Eurasia, made zonal circulation more stable, and reduced the frequency of extreme weather in Suigetsu.

It may be premature to speculate that such an unstable climate

during that period of global warming was analogous to today's apparent increase of extreme weather. However, our data provide additional geological evidence that global climate has discrete modes (=local potential minima) where Holocene, glacial maximum, and future 'hot house earth' (Steffen et al., 2018) are three such examples, with climate becoming more unstable when the system starts to shift between these modes.

5.3. Comparison with speleothem data

The suite of Chinese speleothem records, with Hulu Cave as the most famous example, is often considered as representative of East Asia's palaeoclimate (Cheng et al., 2016; Liu et al., 2020). The millennial scale climate oscillations in the Chinese speleothem records are generally interpreted as counterparts of the known climatic episodes in the circum-N. Atlantic regions (such as D–O and Bond events), and the timings of their occurrences in China are often believed to be synchronous with the N. Atlantic (*e.g.* Wang et al., 2001, 2005). More recently, quantitative assessments of the relative timings between China and Greenland or among speleothems from across the world have been made based on wiggles of cosmogenic isotopes (Adolphi et al., 2018) or absolute U/Th dates (Corrick et al., 2020). They concluded that the millennial scale changes are generally synchronous within errors (but with some exceptions; significant offsets were recognised such as Heinrich 2, GI-11, GI-15.1, and GI-23.1 where ages estimated in different regions do not converge) (Adolphi et al., 2018; Corrick et al., 2020 and references therein). However, many of the absolute ages used for the comparison also had multi-centennial uncertainties, preventing investigation of the more fine-scale 'anatomy' of the spatio-temporal structures of the climatic change.

Looking at the onset of the Lateglacial interstadial (where asynchrony is observed between Suigetsu and NGRIP), the start of the warming transition at Hulu has two steps (Figs. 10D and 12C), of which the later one is indeed (almost exactly) synchronous with the warming in Greenland. The ramp fitting also defines the start of the transition near this point. However, the earlier step agrees better with the abrupt warming in Suigetsu (light blue arrows in Figs. 10D and 12C). In the similarly well age-constrained Yamen, Dongge, and Furong Cave records (Dykoski et al., 2005; Yang et al., 2010; Li et al., 2011), the starts of the transition were, within error, synchronous with Suigetsu, and leading that of NGRIP beyond 1 (Yamen and Dongge) or 2 (Furong) sigma combined error ranges (Fig. 12D-F; Table 3).

Such 'lead to Greenland' is not evident with the ramp midpoints of

those Chinese speleothem records. Instead, the midpoints lag significantly behind Suigetsu, or even Greenland. This is simply because the transitions in the Chinese records are more gradual than in Suigetsu and Greenland. When investigating causal links, however, the start of the change is more important than the midpoint. On the basis of the relative timings of the start points, we propose that the transition to the Lateglacial interstadial in Asia, including both Japan and China, started earlier than in Greenland.

The speleothem record of Bittoo Cave in Northern India shows more abrupt change than in China at the onset of the Lateglacial interstadial (Fig. 12G) (Kathayat et al., 2016). Although the Bittoo record is not as tightly constrained for age as the Chinese speleothems, the abrupt shift is dated around that of Suigetsu (*i.e.* earlier than Greenland). If these observations are indeed the case, then the Indian monsoon and the East Asian monsoon appear to have reacted to the deglaciation as a continuous unit, with Northern India and Japan (where changes were more abrupt) being more closely linked to the mechanism that drove the change, and/or more decoupled from the North Atlantic processes.

The Cariaco Basin record can now be much more robustly correlated with the ice core and speleothem age scales, using the revised estimation of the marine reservoir age (Hughen and Heaton, 2020). Under this new light, the transition in the Cariaco Basin is indeed synchronous (within chronological uncertainty) with Greenland (Fig. 10H), implying that both tropical and Northern Atlantic regions were under the direct influence of the Atlantic meridional overturning circulation (AMOC).

The abrupt transition in the speleothem record from the Pacific coast of South America (El Condor) also shows a significant lag behind Suigetsu (>1 sigma error) and synchrony with Greenland (Fig. 12H) (Cheng et al., 2013). Although it is risky to give too much significance to a single site, this also suggests support for our view that the mechanism that is responsible for the earlier shift in the monsoon regions had its origin nearer to Northern India and/or Japan.

5.4. Mechanisms behind the observed spatio-temporal structure of deglacial climate changes

Our detailed comparison of spatio-temporal structures has unveiled differences among deglacial climatic transitions. The onset of the interstadial was earlier in Japan by about 230 years, and the climate was unstable for several centuries before and after the onset. During the transitional time, after the warming in Japan and before the warming in the North Atlantic, there was a period with much increased frequency of stormy weather. On the other hand, the other abrupt warming at the
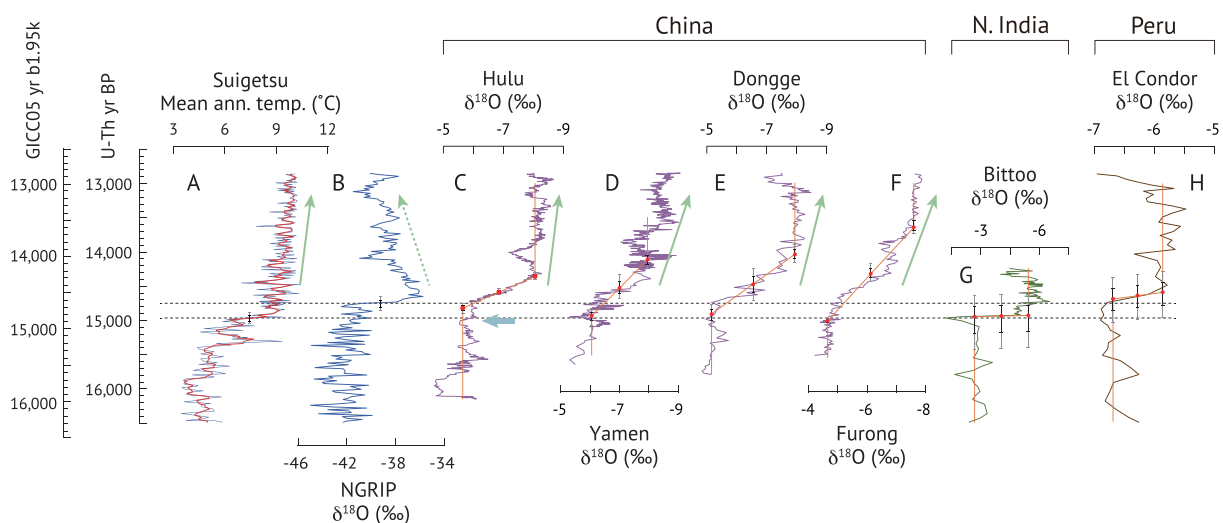
Fig. 12. Onsets of the Lateglacial interstadial in: Suigetsu (A), Greenland (B), and speleothems from across the world (C-H; locations are shown on Fig. 1). Black dotted lines denote transitions in Suigetsu and NGRIP. Error bands show 1 sigma (black) and 2 sigma (grey) uncertainties.

Table 3
Results of the ramp function fitting to the $\delta^{18}O$ data of speleothems in different regions, for the onset of the Lateglacial interstadial (Corrick et al., 2020 and references therein).

	Hulu (H82)				Yamen (Y1)				Dongge (D4)			
	U/Th yr BP	Age error (−1 sigma)	Age error (+1 sigma)	$\delta^{18}O$ (‰)	U/Th yr BP	Age error (−1 sigma)	Age error (+1 sigma)	$\delta^{18}O$ (‰)	U/Th yr BP	Age error (−1 sigma)	Age error (+1 sigma)	$\delta^{18}O$ (‰)
Model end	13,000.0	39.7	38.2	−8.04	13,500.0	122.4	116.6	−7.95	13,000.0	80.0	71.0	−7.94
Ramp end	14,351.7	50.4	47.2	−8.04	14,106.2	111.7	134.1	−7.95	14,031.1	142.4	132.5	−7.94
Ramp midpoint	14,587.3	45.0	40.9	−6.85	14,521.4	198.9	154.8	−7.00	14,470.5	225.7	228.5	−6.55
Ramp start	14,823.0	71.1	73.3	−5.65	14,936.6	100.8	145.5	−6.05	14,909.8	142.2	176.7	−5.16
Model start	16,500.0	43.7	69.6	−5.65	15,500.0	330.1	402.4	−6.05	16,500.0	140.4	123.5	−5.16

	Furong (FR5)				Bittoo (BT1)				Condor (ELC)			
	U/Th yr BP	Age error (−1 sigma)	Age error (+1 sigma)	$\delta^{18}O$ (‰)	U/Th yr BP	Age error (−1 sigma)	Age error (+1 sigma)	$\delta^{18}O$ (‰)	U/Th yr BP	Age error (−1 sigma)	Age error (+1 sigma)	$\delta^{18}O$ (‰)
Model end	13,000.0	70.9	57.2	−7.59	14,230.0	987.9	249.1	−5.42	13,000.0	186.2	114.7	−5.87
Ramp end	13,640.2	208.0	95.0	−7.59	14,917.3	294.8	470.8	−5.42	14,591.9	303.2	358.0	−5.87
Ramp midpoint	14,327.0	158.7	106.5	−6.12	14,929.6	303.2	478.9	−4.05	14,638.4	309.1	350.0	−6.29
Ramp start	15,013.7	42.0	52.1	−4.65	14,941.9	311.6	487.0	−2.68	14,684.9	313.7	338.7	−6.70
Model start	16,500.0	60.8	65.5	−4.65	16,500.0	289.5	184.7	−2.68	16,500.0	470.8	795.3	−6.70

Holocene onset was synchronous in both regions, and there was no particularly stormy transitional period. All things considered, the Lateglacial interstadial can probably be understood as the last D–O event (which itself is subject to further investigation), but the Holocene onset was driven by a different mechanism. In other words, the Holocene cannot be understood as an extended D–O event, and switching on/off of the AMOC alone cannot account for all that happened during the Lateglacial to early Holocene transition.

As a qualitative explanation of what we observe in Greenland, Suigetsu, and other sites, we propose the following scenario (Fig. 13):
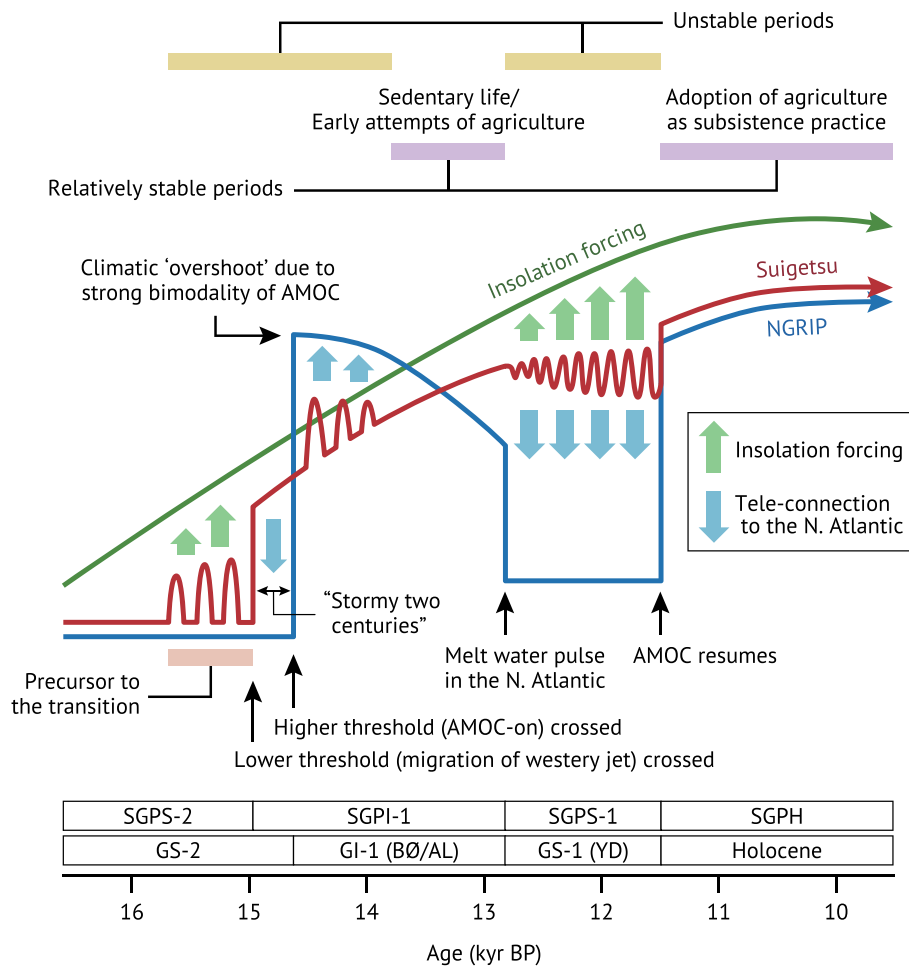
Fig. 13. A schematic explanation of the proposed mechanism that drove temperature transitions and climate stability at Lake Suigetsu (original data: Fig. 9). Climate becomes unstable when insolation forcing and teleconnection to the N. Atlantic operate in opposing directions. Stable climate during the second half of the Lateglacial interstadial and early Holocene may have contributed to major changes in human lifestyles.

Since the initiation of the last deglaciation, boreal high-latitudinal summer insolation kept increasing in a sinusoidal (= gradual) manner, to which the Southern Hemisphere and the tropical regions responded linearly (Fig. 10F, G). In contrast, the Asian Monsoon region that encompasses Northern India, China and Japan had some threshold system that prevented the region from responding linearly to the deglacial insolation forcing. As a mechanism that has strong enough bimodality to generate 'abrupt' change, we propose migration of the westerly jet between the north and the south of the Tibetan plateau (Fig. 14).

Seasonal migration of the westerly jet is common in many regions. However, because the Tibetan plateau and Himalayas act as a topographical barrier, the main axis of the westerly jet over Eurasia has a strong tendency to be positioned either to the south of the Himalayas (winter) or to the north of the Tibetan Plateau (summer), but rarely in between (Schiemann et al., 2009). When the jet 'jumps' to the north, it creates space for the monsoon system to operate, allowing warm and moist oceanic air masses to penetrate into the Chinese and Indian interiors (Liang and Wang, 1998; Sun et al., 2006; Sampe and Xie, 2010). Based on dust analysis of a marine core from the Sea of Japan, Nagashima et al. (2011) postulated that such a bimodal jump of the westerly jet is also analogous to the contrast between stadial and interstadial conditions of the last glacial age. Because Suigetsu is in the region where the climate is directly affected by such a bimodal process (Fig. 14), the jump of the westerly jet can determine whether Japan belongs to the continental or oceanic air masses, and generate abrupt climatic change in Japan. It would be possible to test this hypothesis by analysing the origin of the aeolian dust in sediments, as performed by Nagashima et al. (2011), for a different time window.

While the system was still 'resisting' reaction to the increasing pressure from the orbital forcing, the climate in Japan became unstable (probably the westerly jet was intermittently 'jumping' to the north, allowing warm spikes to occur in Japan). After the threshold was crossed at *ca.* 14.97 IntCal20 kyr BP, the regional climate of East Asia started following the orbital forcing more linearly (Fig. 13) (though with some superimposed complications – see below).

In the North Atlantic regions, the switching on/off of the AMOC operated as a higher threshold that has stronger bimodality than in Asia. Therefore, it took a longer time to respond to the orbital forcing and generated an abrupt and regionally more amplified climatic shift. This 'overshoot' of the climate during the earlier half of the Lateglacial interstadial generated disparity with other regions that responded to the orbital forcing more linearly, which temporarily made the climate in Japan unstable. However, as the AMOC still had not acquired high enough hysteresis (the inertia to stay in its 'on' mode for the longer term within post-glacial boundary conditions), the early interstadial warming swiftly terminated and the climate in the North Atlantic regions started gradually returning to the stadial mode (Ganopolski and Rahmstorf, 2001). During this period of cooling in the N. Atlantic and warming in East Asia, the longitudinal temperature balance was re-established, which helped zonal circulation re-establish and made the climate in Eurasia more stable (Figs. 9B, 13).

The Younger Dryas cold reversal (or GS-1 in a more region-specific context) occurred as a result of the shutting down of the AMOC (of which a meltwater pulse is the most likely trigger), and the amplitude of the change was accordingly greatest in the circum-N. Atlantic regions. Its influence extended to the east through atmospheric teleconnection and reached the Asian Monsoon front. However, Asian regional climate did not cross the threshold again but instead stayed in the 'postglacial-like' mode, as is supported by the relatively small amplitude of the change seen in Suigetsu (and also Hulu, though the difference in signal strength compared to the circum-North Atlantic regions is less evident than Suigetsu). The orbital and N. Atlantic forcing agents operating in opposing directions, however, made the climate in Japan unstable during the cold reversal period (Fig. 13).

When the cold reversal terminated in the N. Atlantic and its influence on Asia through teleconnection was eased, the Asian climate that had already been in its 'postglacial' mode swiftly recovered (*i.e.* the changes in the N. Atlantic and Japan were synchronous) and became stable because the forcing agents stopped counteracting each other. According to the formal stratigraphy, the warm and relatively stable era that continues through to the present (namely the Holocene) started at the end of the Lateglacial cold reversal (Mangerud et al., 1974; Walker et al., 2009). In Asia, however, the onset of the Lateglacial interstadial was the more decisive transition, with the following smaller oscillation (the cold reversal) being only remotely influenced by the N. Atlantic regional processes.

5.5. Implications for human history

Greenland ice core records have been very widely used as a template of past climatic changes even in very remote locations, including west and east Eurasia. To discuss the origins of sedentary life and agriculture in Europe and the Middle East, believed to have their roots in the southern Levant (roughly corresponding to today's Syria, Lebanon, Jordan, Israel, and Palestine), the climato-stratigraphy of Scandinavia and/or Greenland have (despite the large geographical distance) often been invoked (*e.g.* Moore and Hillman, 1992; Robinson et al., 2006). However, the comparison between Greenland and Suigetsu reveals that
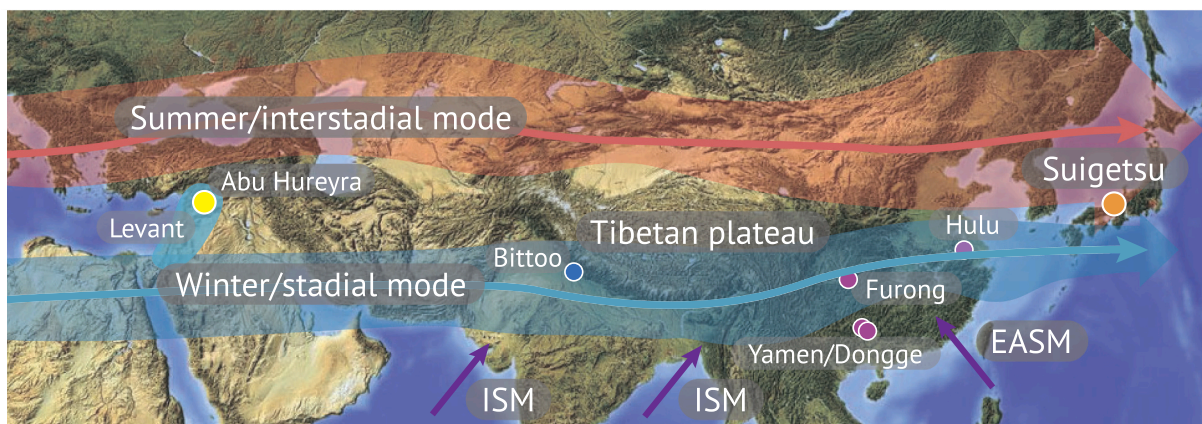

Fig. 14. Typical locations of the westerly jet in summer (red) and winter (blue) in the modern day (modified after Schiemann et al., 2009). The two distinct modes may be analogous to the migration of the westerly jet between stadial and interstadial modes. The Indian summer monsoon (ISM) and the East Asian summer monsoon (EASM), which bring warm and moist air, operate to the south of the westerly jet.

the N. Atlantic exhibits a regional threshold and amplifying mechanism, the influence of which is not pan-hemispheric (at least, it attenuates considerably at the monsoon front). The interaction between two regions with different characters sometimes produced periods of more stable or more unstable climate. In light of this, we attempt to interpret the significant change to the human way of life (often referred to as the 'first agricultural revolution') that occurred during the Lateglacial and early Holocene.

One may argue that using Suigetsu as a reference to discuss what happened in the southern Levant is too speculative. Indeed, the southern Levant and Suigetsu are *ca*. 8300 km apart, and belong to different climate zones. However, the distance between the coring site of NGRIP and the southern Levant is also *ca*. 6000 km, which is not drastically closer (Fig. 1A). Suigetsu and the southern Levant belong to the same latitudinal zone (both are about 35°N), with a similar position relative to the zonal circulation (especially the westerly jet), whereas NGRIP and the southern Levant are latitudinally remote (75°N *vs* 35°N) and belong to different atmospheric circulation cells. Even longitudinally, whether the southern Levant belongs to the same 'block' as the N. Atlantic is highly debatable (*e.g.* Hartman et al., 2016). Palaeoclimate archives that cover the whole of the Lateglacial to early Holocene transition and have a decadal resolution (which is essential to diagnose the stability/instability of climate that would be experienced within human lifetimes) are rare. In the absence of better alternatives in geographically closer regions, it may not be too much of a stretch to use Suigetsu as an additional template for comparison.

The origin of agriculture has a long history of debate (*e.g.* Kuijt and Goring-Morris, 2002; Hartman et al., 2016). Among many hypotheses, that which postulates the role of the Younger Dryas cold reversal as forcing people to increase productivity has attracted the attention of many researchers (*e.g.* Bar-Yosef and Belfer-Cohen, 1992; Moore and Hillman, 1992; Munro, 2003). More recently, however, the ^{14}C ages that were used to support this hypothesis have been re-assessed using modern quality assurance criteria and more developed techniques of age determination. After 'screening' inadequate samples (Blockley and Pinhasi, 2011), calibrating ^{14}C dates using the then latest calibration model, IntCal09 (which is almost identical to the latest model IntCal20 for the period concerned in this interval) (Reimer et al., 2009, 2020), and constraining the ages by Bayesian modelling (Bronk Ramsey, 2009), Blockley and Pinhasi (2011) obtained a much narrower distribution of the ^{14}C dates that clearly indicated that sedentary life and the earliest attempts of agriculture (late Natufian culture) both started during the second half of the Lateglacial interstadial, and that the settlements based mainly on agriculture (Pre-Pottery Neolithic A: PPNA) were established in the very early Holocene. Those were both relatively warm and, more importantly, stable periods. The cold reversal in between those periods, previously thought to have been the period when agriculture was first adopted as a major subsistence practice, proved to have been a period of decline and, instead, a 'cultural gap' (Fig. 9C) (Blockley and Pinhasi, 2011).

One could argue that the elevated temperature of the interstadial and early Holocene was the key to allowing people to practice agriculture. However, this theory cannot explain why people did not commence agriculture earlier (or why late Natufians did not maintain agriculture during the cold reversal) in warmer tropical regions. Similarly, it also remains a mystery why people could start agriculture in multiple locations within only several thousand years after the Holocene onset, whereas agriculture was not practiced in warmer tropical regions for several tens of thousands of years prior to the Holocene onset (Bar-Yosef, 2017).

We propose that the key to answering these questions is in the stability of the climate, rather than the absolute level of temperature (Hartman et al., 2016). The late Natufian and PPNA cultures both prospered during the period where longitudinal temperature disparity was reconciled, zonal circulation was stable, and decadal variability of climate was low (Fig. 9C). When the climate was unstable, on the other

hand, agriculture was too risky a practice for subsistence because it requires 'predictability' of weather for adequate choice of crops. In other words, when prediction was essentially impossible (which was the case when the climate was unstable), agriculture was not even a reasonable choice, regardless of whether the temperature was high or low.

During the second half of the Lateglacial interstadial and early Holocene, the climate of mid-latitudinal Eurasia became 'predictable' for the first time after the last glacial maximum, and agriculture naturally started as a measure that newly became rational, rather than a revolutionary invention of genius. This could also explain why agriculture started independently in many places but exclusively during the Holocene (*e.g.* Batler, 2007; Price and Bar-Yosef, 2011).

Without annually resolved records, it would not be possible to discuss stability or instability of climate because many/most sediments preclude resolving decadal characteristics of climatic change. However, varved sediments make it possible. A good example of such an approach is that of Haug et al. (2003) who analysed the chemical composition of the Cariaco Basin varved sediment and argued that recurring extreme weather (*i.e.* unstable climate) was the key to the decline of the Classic Maya (*ca*. 800 CE). Our hypothesis could be tested if such a study were to be performed in the southern Levant.

6. Conclusions

6.1. Observations

- The onsets of the Holocene were abrupt both in Suigetsu and Greenland, and they were synchronous within 1 sigma errors.
- The onset of the Lateglacial cold reversal in Suigetsu was gradual, whereas that in Greenland (GS-1; regional counterpart of the Younger Dryas) was abrupt. Their start points were synchronous within 1 sigma errors.
- The onsets of the Lateglacial interstadial (GI-1 in Greenland; regional counterpart of the Bølling/Allerød) were abrupt both in Suigetsu and Greenland. However, that in Suigetsu was earlier by *ca*. 2 centuries.
- The onset of the Lateglacial interstadial in China and Northern India were synchronous with Suigetsu, whereas those in the North Atlantic and South America were synchronous with Greenland.
- Climate in Japan was particularly stable during the second half of the Lateglacial interstadial and early Holocene.

6.2. Interpretations

- The Holocene can be seen as an 'extended D–O event' in circum-North Atlantic regions. However, that is not the case in Asia, where the most decisive transition was the onset of the Lateglacial interstadial rather than the Holocene onset.
- During the Lateglacial cold reversal, Asia was under the strong influence of the N. Atlantic, which was the driver of the unstable climate during this period. However, Asia persistently remained in a post-glacial mode after the onset of the Lateglacial interstadial.
- In East and South (and possibly also in West) Asia, the bimodal migration of the westerly jet (which exhibits threshold behaviour because of the Tibetan plateau) is posited as the mechanism to generate abrupt changes.
- Switching on/off of the AMOC has a higher threshold than the N-S migration of the westerly jet. In the N. Atlantic region, it delayed the climatic response to insolation forcing, and amplified the change by strong bimodality.
- The switching of the westerly jet was decoupled from that of the AMOC. When they cross the threshold at different times, a disparity between 'glacial' and 'post-glacial' modes occurs between the N. Atlantic and Asia. The climate in Asia became unstable during intervals of such disparity.

6.3. Hypothesis

- Climatic stability, characteristic of both the second half of the Late-glacial interstadial and early Holocene, was the key for humans to commence sedentary life and adopt agriculture.

Declaration of Competing Interest

None.

Acknowledgements

Appendix A. Supplementary data

Full dataset of pollen counts and reconstructed climates of the Lateglacial to early Holocene part of the SG06 varved sediment core from Lake Suigetsu, Japan, with depth and chronologies. Supplementary data to this article can be found online at [https://doi.org/10.1016/j.gloplacha.2021.103493].

References

Adolphi, F., Bronk Ramsey, C., Erhardt, T., Edwards, R.L., Cheng, H., Turney, C.S.M., Cooper, A., Svensson, A., Rasmussen, S.O., Fischer, H., Muscheler, R., 2018. Connecting the Greenland ice-core and U/Th timescales via cosmogenic radionuclides: testing the synchroneity of Dansgaard–Oeschger events. Clim. Past 14, 1755–1781. https://doi.org/10.5194/cp-14-1755-2018.

Alley, R.B., Marotzke, J., Nordhaus, W.D., Overpeck, J.T., Peteet, D.M., Pielke Jr., R.A., Pierrehumbert, R.T., Rhines, P.B., Stocker, T.F., Talley, L.D., Wallace, J.M., 2003. Abrupt climate change. Science 299 (5615), 2005–2010. https://doi.org/10.1126/science.1081056.

Andersen, K.K., Svensson, A., Johnsen, S.J., Rasmussen, S.O., Bigler, M., Röthlisberger, R., Ruth, U., Siggaard-Andersen, M.-L., Steffensen, J.P., Dahl-Jensen, D., Vinther, B.M., Clausen, H.B., 2006. The Greenland Ice core chronology 2005, 15-42 ka. Part 1: constructing the time scale. Quat. Sci. Rev. 25, 23–24. https://doi.org/10.1016/j.quascirev.2006.08.002.

Bakke, J., Lie, Ø., Heegaard, E., Dokken, T., Haug, G.H., Birks, H.H., Dulski, P., Nilsen, T., 2009. Rapid oceanic and atmospheric changes during the Younger Dryas cold period. Nat. Geosci. 2 (3), 202–205. https://doi.org/10.1038/ngeo439.

Barker, S., Diz, P., Vautravers, M.J., Pike, J., Knorr, G., Hall, I.R., Broecker, W.S., 2009. Interhemispheric Atlantic seesaw response during the last deglaciation. Nature 457, 1097–1102. https://doi.org/10.1038/nature07770.

Bar-Yosef, O., 2017. Multiple origins of agriculture in Eurasia and Africa. In: Tibayrenc, M., Ayala, F.J. (Eds.), On Human Nature -Biology, Psychology, Ethics, Politics, and Religion. Academic Press, Cambridge (USA), pp. 297–331. https://doi.org/10.1016/B978-0-12-420190-3.00019-3.

Bar-Yosef, O., Belfer-Cohen, A., 1992. From foraging to farming in the Mediterranean Levant. In: Gebauer, A.B., Price, T.D. (Eds.), Transitions to Agriculture in Pre-History. Prehistory Press, Madison, pp. 21–48.

Batler, M., 2007. Seeking agriculture's ancient roots. Science 316 (5833), 1830–1835. https://doi.org/10.1126/science.316.5833.1830.

Beck, H.E., Zimmermann, N.E., McVicar, T.R., Vergopolan, N., Berg, A., Wood, E.F., 2018. Present and future Köppen-Geiger climate classification maps at 1-km resolution. Sci. Data 5, 180214. https://doi.org/10.1038/sdata.2018.214.

Behl, R.J., Kennett, J.P., 1996. Brief interstadial events in the Santa Barbara basin, NE Pacific, during the past 60 kyr. Nature 379, 243–246. https://doi.org/10.1038/379243a0.

Björck, S., Walker, M.J.C., Cwynar, L.C., Johnsen, S., Knudsen, K.-L., Lowe, J.J., Wohlfarth, B., INTIMATE Members, 1998. An event stratigraphy for the Last Termination in the North Atlantic region based on the Greenland Ice-core record: a proposal by the INTIMATE group. J. Quat. Sci. 13, 283–292. https://doi.org/10.1002/(SICI)1099-1417(199807/08)13:4<283::AID-JQS386>3.0.CO;2-A.

Blockley, S.P.E., Pinhasi, R., 2011. A revised chronology for the adoption of agriculture in the Southern Levant and the role of Lateglacial climatic change. Quat. Sci. Rev. 30 (1–2), 98–108. https://doi.org/10.1016/j.quascirev.2010.09.021.

Blunier, T., Brook, E.J., 2001. Timing of Millennial-Scale climate Change in Antarctica and Greenland during the Last Glacial Period. Science 291 (5501), 109–112. https://doi.org/10.1126/science.291.5501.109.

Blunier, T., Chappellaz, J., Schwander, J., Dällenbach, A., Stauffer, B., Stocker, T.F., Raynaud, D., Jouzel, J., Clausen, H.B., Hammer, C.U., Johnsen, S.J., 1998. Asynchrony of Antarctic and Greenland climate change during the last glacial period. Nature 394, 739–743. https://doi.org/10.1038/29447.

Brauer, A., Haug, G.H., Dulski, P., Sigman, D.M., Negendank, J.F.W., 2008. An abrupt wind shift in western Europe at the onset of the Younger Dryas cold period. Nat. Geosci. 1, 520–523. https://doi.org/10.1038/ngeo263.

Brauer, A., Hajdas, I., Blockley, S.P.E., Bronk Ramsey, C., Christl, M., Ivy-Ochs, S., Moseley, G.E., Novaczyk, N.N., Rasmussen, S.O., Roberts, H.M., Spötl, C., Staff, R.A, Svensson, A., 2014. The importance of independent chronology in integrating records of past climate change for the 60–8 ka INTIMATE time interval. Quat. Sci. Rev. 106, 47–66. https://doi.org/10.1016/j.quascirev.2014.07.006.

Broecker, W.S., 1998. Paleocean circulation during the last deglaciation: a bipolar seesaw? Paleoceanography 13, 119–121. https://doi.org/10.1029/97PA03707.

Bronk Ramsey, C., 2009. Bayesian analysis of radiocarbon dates. Radiocarbon 51 (1), 337–360. https://doi.org/10.1017/S0033822200033865.

Bronk Ramsey, C., Staff, R.A, Bryant, C.L., Brock, F., Kitagawa, H., van der Plicht, J., Schlolaut, G., Marshall, M.H., Brauer, A., Lamb, H.F., Payne, R.L., Tarasov, P.E., Haraguchi, T., Gotanda, K., Yonenobu, H., Yokoyama, Y., Tada, R., Nakagawa, T., 2012. A complete terrestrial radiocarbon record for 11.2 to 52.8 kyr B.P. Science 338 (6105), 370–374. https://doi.org/10.1126/science.1226660.

Cheng, H., Edwards, R.L., Broecker, W.S., Denton, G.H., Kong, X., Wang, Y., Zhang, R., Wang, X., 2009. Ice age terminations. Science 326 (5950), 248–252. https://doi.org/10.1126/science.1177840.

Cheng, H., Sinha, A., Cruz, F.W., Wang, X., Edwards, R.L., d'Horta, F.M., Ribas, C.C., Vuille, M., Stott, L.D., Auler, A.S., 2013. Climate change patterns in Amazonia and biodiversity. Nat. Commun. 4, 1411. https://doi.org/10.1038/ncomms2415.

Cheng, H., Edwards, R.L., Sinha, A., Spötl, C., Yi, L., Chen, S., Kelly, M., Kathayat, G., Wang, X., Li, X., Kong, X., Wang, Y., Ning, Y., Zhang, H., 2016. The Asian monsoon over the past 640,000 years and ice age terminations. Nature 534, 640–646. https://doi.org/10.1038/nature18591.

Clark, P.U., Pisias, N.G., Stocker, T., Weaver, A., 2002. The role of the thermohaline circulation in abrupt climate change. Nature 415 (6874), 863–869. https://doi.org/10.1038/415863a.

Corrick, C., Drysdale, R.N., Hellstrom, J.C., Capron, E., Rasmussen, S.O., Zhang, X., Fleitmann, D., Couchoud, I., Wolff, E., 2020. Synchronous timing of abrupt climate changes during the last glacial period. Science 369 (6506), 963–969. https://doi.org/10.1126/science.aay5538.

Dykoski, C.A., Edwards, R.L., Cheng, H., Yuan, D., Cai, Y., Zhang, M., Lin, Y., Qing, J., An, Z., Revenaugh, J., 2005. A high-resolution, absolute-dated Holocene and deglacial Asian monsoon record from Dongge Cave, China. Earth Planet. Sci. Lett. 233, 71–86. https://doi.org/10.1016/j.epsl.2005.01.036.

Firestone, R.B., West, A., Kennett, J.P., Becker, L., Bunch, T.E., Revay, Z.S., Schultz, P.H., Belgya, T., Kennett, D.J., Erlandson, J.M., Dickenson, O.J., Goodyear, A.C., Harris, R. S., Howard, G.A., Kloosterman, J.B., Lechler, P., Mayewski, P.A., Montgomery, J., Poreda, R., Darrah, T., Que Hee, S.S., Smith, A.R., Stich, A., Topping, W., Wittke, J. H., Wolbach, W.S., 2007. Evidence for an extraterrestrial impact 12,900 years ago that contributed to the megafaunal extinctions and the Younger Dryas cooling. Proc. Natl. Acad. Sci. 104 (41), 16016–16021. https://doi.org/10.1073/pnas.0706977104.

Fukusawa, H., Koizumi, I., Okamura, M., Yasuda, Y., 1994. Historical earthquake, flood and human activity events recorded in the Holocene sediments of Lake Suigetsu, Fukui Prefecture, Central Japan. J. Geography (Chigaku Zasshi) 103 (2), 127–139 (in Japanese). https://doi.org/10.5026/jgeography.103.2_127.

Ganopolski, A., Rahmstorf, S., 2001. Rapid changes of glacial climate simulated in a coupled climate model. Nature 409, 153–158. https://doi.org/10.1038/35051500.

Goslar, T., Arnold, M., Bard, E., Kuc, T., Pazdur, M.F., Ralska-Jasiwiczowa, M., Rózanski, K., Tisnerat, N., Walanus, A., Wicik, B., Więckowski, K., 1995. High concentration of atmospheric ^{14}C during the Younger Dryas cold episode. Nature 377, 414–417. https://doi.org/10.1038/377414a0.

Gotanda, K., Nakagawa, T., Tarasov, P., Kitagawa, J., Inoue, Y., Yasuda, Y., 2002. Biome classification from Japanese pollen data: application to modern-day and Late Quaternary samples. Quat. Sci. Rev. 21 (4–6), 647–657. https://doi.org/10.1016/S0277-3791(01)00046-4.

Guiot, J., 1990. Methodology of the last climatic cycle reconstruction in France from pollen data. Palaeogeogr. Palaeoclimatol. Palaeoecol. 80 (1), 49–69. https://doi.org/10.1016/0031-0182(90)90033-4.

Hartman, G., Bar-Yosef, O., Brittingham, A., Grosman, L., Munro, N.D., 2016. Hunted gazelles evidence cooling, but not drying, during the Younger Dryas in the southern

Levant. Proc. Natl. Acad. Sci. 113 (15), 3997–4002. https://doi.org/10.1073/pnas.1519862113.

Haug, G.H., Günther, D., Peterson, L.C., Sigman, D.M., Hughen, K.A., Aeschlimann, B., 2003. Climate and the collapse of maya civilization. Science 299 (5613), 1731–1735. https://doi.org/10.1126/science.1080444.

Hoffmann, D.L., Beck, J.W., Richards, D.A., Smart, P.L., Singarayer, J.S., Ketchmark, T., Hawkesworth, C.J., 2010. Towards radiocarbon calibration beyond 28 ka using speleothems from the Bahamas. Earth Planet. Sci. Lett. 289, 1–10. https://doi.org/10.1016/j.epsl.2009.10.004.

Hughen, K.A., Heaton, T.J., 2020. Updated Cariaco Basin ^{14}C calibration dataset from 0–60 cal kyr BP. Radiocarbon 62 (4), 1001–1043. https://doi.org/10.1017/RDC.2020.53.

Hughen, K.A., Overpeck, J.T., Peterson, L.C., Trumbore, S., 1996. Rapid climate changes in the tropical Atlantic region during the last deglaciation. Nature 380, 51–54. https://doi.org/10.1038/380051a0.

Hughen, K.A., Overpeck, J.T., Lehman, S.J., Kashgarian, M., Southon, J., Peterson, L.C., Alley, R., Sigman, D.M., 1998. Deglacial changes in ocean circulation from an extended radiocarbon calibration. Nature 391, 65–68. https://doi.org/10.1038/34150.

Hughen, K.A., Southon, J.R., Lehman, S.J., Overpeck, J.T., 2000. Synchronous radiocarbon and climate Shifts during the last deglaciation. Science 290 (5498), 1951–1954. https://doi.org/10.1126/science.290.5498.1951.

Hughen, K.A., Lehman, S., Southon, J., Overpeck, J., Marchal, O., Herring, C., Turnbull, J., 2004. ^{14}C activity and global carbon cycle changes over the past 50,000 years. Science 303 (5655), 202–207. https://doi.org/10.1126/science.1090300.

Hughen, K., Southon, J., Lehman, S., Bertrand, C., Turnbull, J., 2006. Marine-derived ^{14}C calibration and activity record for the past 50,000 years updated from the Cariaco Basin. Quat. Sci. Rev. 25 (23–24), 3216–3227. https://doi.org/10.1016/j.quascirev.2006.03.014.

Kathayat, G., Cheng, H., Sinha, A., Spötl, C., Edwards, R.L., Zhang, H., Li, X., Yi, L., Ning, Y., Cai, Y., Lui, W., Breitenbach, S.F.M., 2016. Indian monsoon variability on millennial-orbital timescales. Sci. Rep. 6, 24374. https://doi.org/10.1038/srep24374.

Kennett, D.J., Kennett, J.P., West, A., Mercer, C., Que Hee, S.S., Bement, L., Bunch, T.E., Sellers, M., Wolbach, W.S., 2009. Nanodiamonds in the Younger Dryas Boundary Sediment Layer. Science 323 (5910), 94. https://doi.org/10.1126/science.1162819.

Kitaba, I., Nakagawa, T., 2017. Black ceramic spheres as marker grains for microfossil analyses, with improved chemical, physical, and optical properties. Quat. Int. 455, 166–169. https://doi.org/10.1016/j.quaint.2017.08.052.

Kitagawa, H., van der Plicht, J., 1998a. Atmospheric radiocarbon calibration to 45,000 yr BP: late Glacial fluctuations and cosmogenic isotope production. Science 279 (5354), 1187–1190. https://doi.org/10.1126/science.279.5354.1187.

Kitagawa, H., van der Plicht, J., 1998b. A 40,000-Year varve chronology from Lake Suigetsu, Japan: extension of the ^{14}C calibration curve. Radiocarbon 40 (1), 505–515. https://doi.org/10.1017/S0033822200018385.

Kitagawa, H., van der Plicht, J., 2000. Atmospheric radiocarbon calibration beyond 11,900 cal BP from Lake Suigetsu laminated sediments. Radiocarbon 42 (3), 370–381. https://doi.org/10.1017/S0033822200030319.

Kuijt, I., Goring-Morris, N., 2002. Foraging, farming, and social complexity in the Pre-Pottery Neolithic of the Southern Levant: a review and synthesis. J. World Prehist. 16, 361–440. https://doi.org/10.1023/A:1022973114090.

Lane, C.S., Brauer, A., Blockley, S.P.E., Dulski, P., 2013. Volcanic ash reveals time-transgressive abrupt climate change during the Younger Dryas. Geology 41 (12), 1251–1254. https://doi.org/10.1130/G34867.1.

Laskar, J., Robutel, P., Joutel, F., Gastineau, M., Correia, A.C.M., Levrard, B., 2004. A long-term numerical solution for the insolation quantities of the Earth. Astron. Astrophys. 428 (1), 261–285. https://doi.org/10.1051/0004-6361:20041335.

Li, T., Shen, C., Li, H., Li, J., Chiang, H., Song, S., Yuan, D., Lin, C.D.-J., Gao, P., Zhou, J., Wang, J., Ye, M., Tang, L., Xie, S., 2011. Oxygen and carbon isotopic systematics of aragonite speleothems and water in Furong Cave, Chongqing, China. Geochim. Cosmochim. Acta 75, 4140–4156. https://doi.org/10.1016/j.gca.2011.04.003.

Liang, X.Z., Wang, W.C., 1998. Associations between China monsoon rainfall and tropospheric jets. Q. J. R. Meteorol. Soc. 124, 2597–2623. https://doi.org/10.1002/qj.49712455204.

Liu, G., Li, X., Chiang, H.-W., Cheng, H., Yuan, S., Chawchai, S., He, S., Lu, Y., Aung, L.T., Maung, P.M., Tun, W.N., Oo, K.M., Wang, X., 2020. On the glacial-interglacial variability of the Asian monsoon in speleothem δ^{18}O records. Sci. Adv. 6 (7) https://doi.org/10.1126/sciadv.aay8189 eaay8189.

Lowe, J.J., Hoek, W.Z., INTIMATE group, 2001. Inter-regional correlation of palaeoclimatic records for the Last Glacial–Interglacial transition: a protocol for improved correlation recommended by the INTIMATE project group. Quat. Sci. Rev. 20 (11), 1175–1187. https://doi.org/10.1016/S0277-3791(00)00183-9.

Lowe, J.J., Rasmussen, S.O., Björck, S., Hoek, W.Z., Steffensen, J.P., Walker, M.J.C., Yu, Z.C., the INTIMATE Group, 2008. Synchronisation of palaeoenvironmental events in the North Atlantic region during the Last Termination: a revised protocol recommended by the INTIMATE group. Quat. Sci. Rev. 27 (1–2), 6–17. https://doi.org/10.1016/j.quascirev.2007.09.016.

Mangerud, J., Andersen, S.T., Berglund, B.E., Donner, J.J., 1974. Quaternary stratigraphy of Norden, a proposal for terminology and classification. Boreas 3 (3), 109–126. https://doi.org/10.1111/j.1502-3885.1974.tb00669.x.

Mangerud, J., Gulliksen, S., Larsen, E., 2010. ^{14}C-dated fluctuations of the western flank of the Scandinavian Ice Sheet 45–25 kyr BP compared with Bølling–Younger Dryas fluctuations and Dansgaard–Oeschger events in Greenland. Boreas 39 (2), 328–342. https://doi.org/10.1111/j.1502-3885.2009.00127.x.

Marshall, M., Schlolaut, G., Nakagawa, T., Lamb, H., Brauer, A., Staff, R, Bronk Ramsey, C., Tarasov, P., Gotanda, K., Haraguchi, T., Yokoyama, Y., Yonenobu, H.,

Tada, R., Suigetsu 2006 Project Members, 2012. A novel approach to varve counting using μXRF and X-radiography in combination with thin-section microscopy, applied to the Late Glacial chronology from Lake Suigetsu, Japan. Quat. Geochronol. 13, 70–80. https://doi.org/10.1016/j.quageo.2012.06.002.

Moore, A.M.T., Hillman, G.C., 1992. The Pleistocene to Holocene transition and human economy in Southwest Asia: the impact of the Younger Dryas. Am. Antiq. 57 (3), 482–494. https://doi.org/10.2307/280936.

Moore, A.M.T., Kennett, J.P., Napier, W.M., Bunch, T.E., Weaver, J.C., LeCompte, M., Adedeji, A.V., Hackley, P., Kletetschka, G., Hermes, R.E., Wittke, J.H., Razink, J.J., Gaultois, M.W., West, A., 2020. Evidence of cosmic impact at Abu Hureyra, Syria at the Younger Dryas Onset (~12.8 ka): high-temperature melting at >2200°C. Sci. Rep. 10, 4185. https://doi.org/10.1038/s41598-020-60867-w.

Munro, N.D., 2003. Small game, the younger dryas, and the transition to agriculture in the southern levant. Mitteilungen der Gesellschaft für Urgeschichte 12, 47–71.

Muscheler, R., Adolphi, F., Knudsen, M.F., 2014. Assessing the differences between the IntCal and Greenland ice-core time scales for the last 14,000 years via the common cosmogenic radionuclide variations. Quat. Sci. Rev. 106, 81–87. https://doi.org/10.1016/j.quascirev.2014.08.017.

Nagashima, K., Tada, R., Tani, A., Sun, Y., Isozaki, Y., Toyoda, S., Hasegawa, H., 2011. Millennial-scale oscillations of the westerly jet path during the last glacial period. J. Asian Earth Sci. 40, 1214–1220. https://doi.org/10.1016/j.jseaes.2010.08.010.

Nakagawa, T., Brugiapaglia, E., Digerfeldt, G., Reille, M., de Beaulieu, J.-L., Yasuda, Y., 1998. Dense-media separation as a more efficient pollen extraction method for use with organic sediment/deposit samples: comparison with the conventional method. Boreas 27 (1), 15–24. https://doi.org/10.1111/j.1502-3885.1998.tb00864.x.

Nakagawa, T., Tarasov, P.E., Nishida, K., Gotanda, K., Yasuda, Y., 2002. Quantitative pollen-based climate reconstruction in Central Japan: application to surface and Late Quaternary spectra. Quat. Sci. Rev. 21 (18–19), 2099–2113. https://doi.org/10.1016/S0277-3791(02)00014-8.

Nakagawa, T., Kitagawa, H., Yasuda, Y., Tarasov, P.E., Nishida, K., Gotanda, K., Sawai, Y., Yangtze River Civilization Program Members, 2003. Asynchronous climate changes in the North Atlantic and Japan during the last termination. Science 299 (5607), 688–691. https://doi.org/10.1126/science.1078235.

Nakagawa, T., Kitagawa, H., Yasuda, Y., Tarasov, P.E., Gotanda, K., Sawai, Y., 2005. Pollen/event stratigraphy of the varved sediment of Lake Suigetsu, Central Japan from 15,701 to 10,217 SG vyr BP (Suigetsu varve years before present): description, interpretation, and correlation with other regions. Quat. Sci. Rev. 24 (14–15), 1691–1701. https://doi.org/10.1016/j.quascirev.2004.06.022.

Nakagawa, T., Tarasov, P.E., Kitagawa, H., Yasuda, Y., Gotanda, K., 2006. Seasonally specific responses of the East Asian monsoon to deglacial climate changes. Geology 34 (7), 521–524. https://doi.org/10.1130/G21764.1.

Nakagawa, T., Gotanda, K., Haraguchi, T., Danhara, T., Yonenobu, H., Brauer, A., Yokoyama, Y., Tada, R., Takemura, K., Staff, R.A, Payne, R., Bronk Ramsey, C., Bryant, C., Brock, F., Schlolaut, G., Marshall, M., Tarasov, P., Lamb, H., Suigetsu 2006 Project Members, 2012. SG06, a fully continuous and varved sediment core from Lake Suigetsu, Japan: stratigraphy and potential for improving the radiocarbon calibration model and understanding of late Quaternary climate changes. Quat. Sci. Rev. 36, 164–176. https://doi.org/10.1016/j.quascirev.2010.12.013.

Nakagawa, T., Kitagawa, H., Payne, R., Tarasov, P., Demske, D., 2013. A standard sample method for controlling microfossil data precision: a proposal for higher data quality and greater opportunities for collaboration. Quat. Int. 290, 239–244. https://www.sciencedirect.com/science/article/pii/S1040618212033009.

Partin, J.W., Cobb, K.M., Adkins, J.F., Clark, B., Fernandez, D.P., 2007. Millennial-scale trends in West Pacific warm pool hydrology since the Last Glacial Maximum. Nature 449, 452–455. https://doi.org/10.1038/nature06164.

Pedro, J.B., Bostock, H.C., Bitz, C.M., He, F., Vandergoes, M.J., Steig, E.J., Chase, B.M., Krause, C.E., Rasmussen, S.O., Markle, B.R., Cortese, G., 2015. The spatial extent and dynamics of the Antarctic Cold Reversal. Nat. Geosci. 9, 51–55. https://doi.org/10.1038/ngeo2580.

Peterson, L.C., Haug, G.H., Hughen, K.A., Röhl, U., 2000. Rapid changes in the hydrologic cycle of the Tropical Atlantic during the last glacial. Science 290 (5498), 1947–1951. https://doi.org/10.1126/science.290.5498.1947.

Price, T.D., Bar-Yosef, O., 2011. The origins of agriculture: new data, new ideas: an introduction to supplement 4. Curr. Anthropol. 52 (S4), 163–174. https://doi.org/10.1086/659964.

Rach, O., Brauer, A., Wilkes, H., Sachse, D., 2014. Delayed hydrological response to Greenland cooling at the onset of the Younger Dryas in western Europe. Nat. Geosci. 7 (2), 109–112. https://doi.org/10.1038/ngeo2053.

Rasmussen, S.O., Andersen, K.K., Svensson, A.M., Steffensen, J.P., Vinther, B.M., Clausen, H.B., Siggaard-Andersen, M.-L., Johnsen, S.J., Larsen, L.B., Dahl-Jensen, D., Bigler, M., Röthlisberger, R., Fischer, H., Goto-Azuma, K., Hansson, M.E., Ruth, U., 2006. A new Greenland ice core chronology for the last glacial termination. J. Geophys. Res. 111, D06102 https://doi.org/10.1029/2005JD006079.

Rasmussen, S.O., Bigler, M., Blockley, S.P., Blunier, T., Buchardt, S.L., Clausen, H.B., Cvijanovic, I., Dahl-Jensen, D., Johnsen, S.J., Fischer, H., Gkinis, V., Guillevic, M., Hoek, W.Z., Lowe, J.J., Pedro, J.B., Popp, T., Seierstad, I.K., Steffensen, J.P., Svensson, A.M., Vallelonga, P., Vinther, B.M., Walker, M.J.C., Wheatley, J.J., Winstrup, M., 2014. A stratigraphic framework for abrupt climatic changes during the Last Glacial period based on three synchronized Greenland ice-core records: refining and extending the INTIMATE event stratigraphy. Quat. Sci. Rev. 106, 14–28. https://doi.org/10.1016/j.quascirev.2014.09.007.

Raymo, M.E., 1997. The timing of major climate terminations. Paleoceanography 12 (4), 577–585. https://doi.org/10.1029/97PA01169.

Reimer, P.J., Baillie, M.G.L., Bard, E., Bayliss, A., Beck, J.W., Bertrand, C.J.H., Blackwell, P.G., Buck, C.E., Burr, G.S., Cutler, K.B., Damon, P.E., Edwards, R.L., Fairbanks, R.G., Friedrich, M., Guilderson, T.P., Hogg, A.G., Hughen, K.A.,

Kromer, B., McCormac, G., Manning, S., Bronk Ramsey, C., Reimer, R.W., Remmele, S., Southon, J.R., Stuiver, M., Talamo, S., Taylor, F.W., van der Plicht, J., Weyhenmeyer, C.E., 2004. IntCal04 terrestrial radiocarbon age calibration, 0-26 cal kyr BP. Radiocarbon 46 (3), 1029–1058. https://doi.org/10.1017/S0033822200032999.

Reimer, P.J., Baillie, M.G.L., Bard, E., Bayliss, A., Beck, J.W., Blackwell, P.G., Bronk Ramsey, C., Buck, C.E., Burr, G.S., Edwards, R.L., Friedrich, M., Grootes, P.M., Guilderson, T.P., Hajdas, I., Heaton, T.J., Hogg, A.G., Hughen, K.A., Kaiser, K.F., Kromer, B., McCormac, F.G., Manning, S.W., Reimer, R.W., Richards, D.A., Southon, J.R., Talamo, S., Turney, C.S.M., van der Plicht, J., Weyhenmeyer, C.E., 2009. INTCAL09 and Marine09 Radiocarbon age calibration curves, 0-50,000 years CAL BP. Radiocarbon 51 (4), 1111–1150. https://doi.org/10.1017/S0033822200034202.

Reimer, P.J., Bard, E., Bayliss, A., Beck, J.W., Blackwell, P.G., Bronk Ramsey, C., Buck, C.E., Cheng, H., Edwards, R.L., Friedrich, M., Grootes, P.M., Guilderson, T.P., Haflidason, H., Hajdas, I., Hatté, C., Heaton, T.J., Hoffmann, D.L., Hogg, A.G., Hughen, K.A., Kaiser, K.F., Kromer, B., Manning, S.W., Niu, M., Reimer, R.W., Richards, D.A., Scott, E.M., Southon, J.R., Staff, R.A., Turney, C.S.M., van der Plicht, J., 2013. IntCal13 and Marine13 Radiocarbon Age Calibration Curves 0–50,000 Years cal BP. Radiocarbon 55 (4). https://doi.org/10.2458/azu_js_rc.55.16947.

Reimer, P.J., Austin, W.E.N., Bard, E., Bayliss, A., Blackwell, P.G., Bronk Ramsey, C., Butzin, M., Cheng, H., Edwards, R.L., Friedrich, M., Grootes, P.M., Guilderson, T.P., Hajdas, I., Heaton, T.J., Hogg, A.G., Hughen, K.A., Kromer, B., Manning, S.W., Muscheler, R., Palmer, J.G., Pearson, C., van der Plicht, J., Reimer, R.W., Richards, D.A., Scott, E.M., Southon, J.R., Turney, C.S.M., Wacker, L., Adolphi, F., Büntgen, U., Capano, M., Fahrni, S.M., Fogtmann-Schulz, A., Friedrich, R., Köhler, P., Kudsk, S., Miyake, F., Olsen, J., Reinig, F., Sakamoto, M., Sookdeo, A., Talamo, S., 2020. The IntCal20 Northern hemisphere radiocarbon age calibration Curve (0–55 cal kBP). Radiocarbon 62 (4), 725–757. https://doi.org/10.1017/RDC.2020.41.

Robinson, S.A., Black, S., Sellwood, B.W., Valdes, P.J., 2006. A review of palaeoclimates and palaeoenvironments in the Levant and Eastern Mediterranean from 25,000 to 5000 years BP: setting the environmental background for the evolution of human civilisation. Quat. Sci. Rev. 25, 1517–1541. https://doi.org/10.1016/j.quascirev.2006.02.006.

Sampe, T., Xie, S.-P., 2010. Large-scale dynamics of the Meiyu–Baiu Rainband: environmental Forcing by the Westerly Jet. J. Clim. 23, 113–134. https://doi.org/10.1175/2009JCLI3128.1.

Schiemann, R., Lüthi, D., Schär, C., 2009. Seasonality and interannual variability of the Westerly Jet in the Tibetan Plateau Region. J. Clim. 22, 2940–2957. https://doi.org/10.1175/2008JCLI2625.1.

Schlolaut, G., Marshall, M.H., Brauer, A., Nakagawa, T., Lamb, H.F., Staff, R.A, Bronk Ramsey, C., Bryant, C.L., Brock, F., Kossler, A., Tarasov, P.E., Yokoyama, Y., Tada, R., Haraguchi, T., Suigetsu 2006 project members, 2012. An automated method for varve interpolation and its application to the Late Glacial chronology from Lake Suigetsu, Japan. Quat. Geochronol. 13, 52–69. https://doi.org/10.1016/j.quageo.2012.07.005.

Schlolaut, G., Brauer, A., Marshall, M.H., Nakagawa, T., Staff, R.A, Bronk Ramsey, C., Lamb, H.F., Bryant, C.L., Naumann, R., Dulski, P., Brock, F., Yokoyama, Y., Tada, R., Haraguchi, T., Suigetsu 2006 project members, 2014. Event layers in the Japanese Lake Suigetsu 'SG06' sediment core: description, interpretation and climatic implications. Quat. Sci. Rev. 83, 157–170. https://doi.org/10.1016/j.quascirev.2013.10.026.

Schlolaut, G., Brauer, A., Nakagawa, T., Lamb, H.F., Tyler, J., Staff, R.A, Marshall, M.H., Bronk Ramsey, C., Bryant, C.L., Tarasov, P.E., 2017. Evidence for a bi-partition of the Younger Dryas Stadial in East Asia associated with inversed climate characteristics compared to Europe. Sci. Rep. 7, 44983. https://doi.org/10.1038/srep44983.

Schlolaut, G., Staff, R.A, Brauer, A., Lamb, H.F., Marshall, M.H., Bronk Ramsey, C., Nakagawa, T., 2018. An extended and revised Lake Suigetsu varve chronology from ~50 to ~10 ka BP based on detailed sediment micro-facies analyses. Quat. Sci. Rev. 200, 351–366. https://doi.org/10.1016/j.quascirev.2018.09.021.

Shen, C.-C., Kano, A., Hori, M., Lin, K., Chiu, T.-C., Burre, G.S., 2010. East Asian monsoon evolution and reconciliation of climate records from Japan and Greenland during the last deglaciation. Quat. Sci. Rev. 29 (23–24), 3327–3335. https://doi.org/10.1016/j.quascirev.2010.08.012.

Sigl, M., Fudge, T.J., Winstrup, M., Cole-Dai, J., Ferris, D., McConnell, J.R., Taylor, K.C., Welten, K.C., Woodruff, T.E., Adolphi, F., Bisiaux, M., Brook, E.J., Buizert, C., Caffee, M.W., Dunbar, N.W., Edwards, R., Geng, L., Iverson, N., Koffman, B., Layman, L., Maselli, O.J., McGwire, K., Muscheler, R., Nishiizumi, K., Pasteris, D.R., Rhodes, R.H., Sowers, T.A., 2016. The WAIS divide deep ice core WD2014 chronology – part 2: Annual-layer counting (0–31 ka BP). Clim. Past 12, 769–786. https://doi.org/10.5194/cp-12-769-2016.

Southon, J., Noronha, A.L., Cheng, H., Edwards, R.L., Wang, Y., 2012. A high-resolution record of atmospheric ¹⁴C based on Hulu Cave speleothem H82. Quat. Sci. Rev. 33, 32–41. https://doi.org/10.1016/j.quascirev.2011.11.022.

Staff, R.A., Bronk Ramsey, C., Nakagawa, T., Suigetsu 2006 Project Members, 2010. A re-analysis of the Lake Suigetsu terrestrial radiocarbon calibration dataset. Nucl. Inst. Methods Phys. Res. B 268 (7–8), 960–965. https://doi.org/10.1016/j.nimb.2009.10.074.

Staff, R.A., Bronk Ramsey, C., Bryant, C.L., Brock, F., Payne, R.L., Schlolaut, G., Marshall, M.H., Brauer, A., Lamb, H.F., Tarasov, P., Yokoyama, Y., Haraguchi, T., Gotanda, K., Yonenobu, H., Nakagawa, T., 2011. New ¹⁴C Determinations from Lake Suigetsu, Japan: 12,000 to 0 Cal BP. Radiocarbon. 53 (3), 511–528. https://doi.org/10.1017/S0033822200034627.

Staff, R.A., Nakagawa, T., Schlolaut, G., Marshall, M.H., Brauer, A., Lamb, H.F., Bronk Ramsey, C., Bryant, C.L., Brock, F., Kitagawa, H., van der Plicht, J., Payne, R.L., Smith, V.C., Mark, D.F., Macleod, A., Blockley, S.P.E., Schwenninger, J.-L., Tarasov, P.E., Haraguchi, T., Gotanda, K., Yonenobu, H., Yokoyama, Y., Suigetsu 2006 Project Members, 2013a. The multiple chronological techniques applied to the Lake Suigetsu SG06 sediment core, Central Japan. Boreas 42, 259–266. https://doi.org/10.1111/j.1502-3885.2012.00278.x.

Staff, R.A., Schlolaut, G., Bronk Ramsey, C., Brock, F., Bryant, C.L., Kitagawa, H., van der Plicht, J., Marshall, M.H., Brauer, A., Lamb, H.F., Payne, R.L., Tarasov, P.E., Haraguchi, T., Gotanda, K., Yonenobu, H., Yokoyama, Y., Nakagawa, T., 2013b. Integration of the Old and New Lake Suigetsu (Japan) terrestrial radiocarbon calibration data sets. Radiocarbon 55 (4), 2049–2058. https://doi.org/10.2458/azu_js_rc.v55i2.16339.

Steffen, W., Rockström, J., Richardson, K., Lenton, T.M., Folke, C., Liverman, D., Summerhayes, C.P., Barnosky, A.D., Cornell, S.E., Crucifix, M., Donges, J.F., Fetzer, I., Lade, S.J., Scheffer, M., Winkelmann, R., Schellnhuber, H.J., 2018. Trajectories of the Earth System in the Anthropocene. Proc. Natl. Acad. Sci. 115 (33), 8252–8259. https://doi.org/10.1073/pnas.1810141115.

Steffensen, J.P., Andersen, K.K., Bigler, M., Clausen, H.B., Dahl-Jensen, D., Fischer, H., Goto-Azuma, K., Hansson, M., Johnsen, S.J., Jouzel, J., Masson-Delmotte, V., Popp, T., Rasmussen, S.O., Röthlisberger, R., Ruth, U., Stauffer, B., Siggaard-Andersen, M.-L., Sveinbjörnsdóttir, Á.E., Svensson, A., White, J.W.C., 2008. High-resolution Greenland Ice core data show abrupt climate change happens in few years. Science 321 (5889), 680–684. https://doi.org/10.1126/science.1157707.

Stocker, T.F., Johnsen, S.J., 2003. A minimum thermodynamic model for the bipolar seesaw. Paleoceanography 18, 1087. https://doi.org/10.1029/2003PA000920.

Stuiver, M., Reimer, P.J., Bard, E., Beck, J.W., Burr, G.S., Hughen, K.A., Kromer, B., McCormac, G., van der Plicht, J., Spurk, M., 1998. INTCAL98 radiocarbon age calibration, 24,000-0 cal BP. Radiocarbon 40 (3), 1041–1083. https://doi.org/10.1017/S0033822200019123.

Sun, Y., Chen, J., Clemens, S.C., Liu, Q., Ji, J., Tada, R., 2006. East Asian monsoon variability over the last seven glacial cycles recorded by a loess sequence from the northwestern Chinese Loess Plateau. Geochem. Geophys. Geosyst. 7 (12) https://doi.org/10.1029/2006GC001287. Q12Q02.

Suzuki, Y., Tada, R., Yamada, K., Irino, T., Nagashima, K., Nakagawa, T., Omori, T., 2016. Mass accumulation rate of detrital materials in Lake Suigetsu as a potential proxy for heavy precipitation: a comparison of the observational precipitation and sedimentary record. Progr. Earth Planet. Sci. 3, 5. https://doi.org/10.1186/s40645-016-0081-x.

Svensson, A., Andersen, K.K., Bigler, M., Clausen, H.B., Dahl-Jensen, D., Davies, S.M., Johnsen, S.J., Muscheler, R., Rasmussen, S.O., Röthlisberger, R., Steffensen, J.P., Vinther, B.M., 2006. The Greenland Ice Core Chronology 2005, 15-42 ka. Part 2: comparison to other records. Quat. Sci. Rev. 25, 23–24. https://doi.org/10.1016/j.quascirev.2006.08.003.

Svensson, A., Dahl-Jensen, D., Steffensen, J.P., Blunier, T., Rasmussen, S.O., Vinther, B. M., Vallelonga, P., Capron, E., Gkinis, V., Cook, E., Kjær, H.A., Muscheler, R., Kipfstuhl, S., Wilhelms, F., Stocker, T.F., Fischer, H., Adolphi, F., Erhardt, T., Sigl, M., Landais, A., Parrenin, F., Buizert, C., McConnell, J.R., Severi, M., Mulvaney, R., Bigler, M., 2020. Bipolar volcanic synchronization of abrupt climate change in Greenland and Antarctic ice cores during the last glacial period. Clim. Past 16, 1565–1580. https://doi.org/10.5194/cp-16-1565-2020.

Tarasov, P.E., Nakagawa, T., Demske, D., Österle, H., Igarashi, Y., Kitagawa, J., Mokhova, L., Bazarova, V., Okuda, M., Gotanda, K., Miyoshi, N., Fujiki, T., Takemura, K., Yonenobu, H., Fleck, A., 2011. Progress in the reconstruction of Quaternary climate dynamics in the Northwest Pacific: A new modern analogue reference dataset and its application to the 430-kyr pollen record from Lake Biwa. Earth-Sci. Rev. 108 (1–2), 64–79. https://doi.org/10.1016/j.earscirev.2011.06.002.

van der Plicht, J., Beck, J.W., Bard, E., Baillie, M.G.L., Blackwell, P.G., Buck, C.E., Friedrich, M., Guilderson, T.P., Hughen, K.A., Kromer, B., McCormac, F.G., Bronk Ramsey, C., Reimer, P.J., Reimer, R.W., Remmele, S., Richards, D.A., Southon, J.R., Stuiver, M., Weyhenmeyer, C.E., 2004. NotCal04 – Comparison/ calibration C-14 records 26-50 cal kyr BP. Radiocarbon 46 (3), 1225–1238. https://doi.org/10.1017/S0033822200033117.

Vinther, M., Clausen, H.B., Johnsen, S.J., Rasmussen, S.O., Andersen, K.K., Buchardt, S. L., Dahl-Jensen, D., Seierstad, I.K., Siggaard-Andersen, M.-L., Steffensen, J.P., Svensson, A., Olsen, J., Heinemeier, J., 2006. A synchronized dating of three Greenland ice cores throughout the Holocene. J. Geophys. Res. 111, D13102 https://doi.org/10.1029/2005JD006921.

WAIS Divide Project Members, 2013. Onset of deglacial warming in West Antarctica driven by local orbital forcing. Nature 500, 440–444. https://doi.org/10.1038/nature12376.

Walker, M., Johnsen, S., Rasmussen, S.O., Popp, T., Steffensen, J.-P., Gibbard, P., Hoek, W., Lowe, J., Andrews, J., Björck, S., Cwynar, L.C., Hughen, K., Kershaw, P., Kromer, B., Litt, T., Lowe, D.J., Nakagawa, T., Newnham, R., Schwander, J., 2009. Formal definition and dating of the GSSP (Global Stratotype Section and Point) for the base of the Holocene using the Greenland NGRIP ice core, and selected auxiliary records. J. Quat. Sci. 24 (1), 3–17. https://doi.org/10.1002/jqs.1227.

Wang, Y.J., Cheng, H., Edwards, R.L., An, Z.S., Wu, J.Y., Shen, C.-C., Dorale, J.A., J.A., 2001. A High-Resolution Absolute-Dated late Pleistocene Monsoon Record from Hulu Cave, China. Science 294 (5550), 2345–2348. https://doi.org/10.1126/science.1064618.

Wang, Y., Cheng, H., Edwards, R.L., He, Y., Kong, X., An, Z., Wu, J., Kelly, M.J., Dykoski, C.A., Li, X., 2005. The Holocene Asian Monsoon: Links to Solar changes and North Atlantic climate. Science 308 (5723), 854–857. https://doi.org/10.1126/science.1106296.

Wang, Y., Cheng, H., Edwards, R.L., Kong, X., Shao, X., Chen, S., Wu, J., Jiang, X., Wang, X., An, Z., 2008. Millennial- and orbital-scale changes in the East Asian monsoon over the past 224,000 years. Nature 451, 1090–1093. https://doi.org/10.1038/nature06692.

Yang, Y., Yuan, D., Cheng, H., Zhang, M., Qin, J., Lin, Y., Zhu, X., Edwards, R.L., 2010. Precise dating of abrupt shifts in the Asian Monsoon during the last deglaciation based on stalagmite data from Yamen Cave, Guizhou Province, China. Sci. China Earth Sci. 53 (5), 633–641. https://doi.org/10.1007/s11430-010-0025-z.

Yoshioka, K., 1973. Plant Geography. Kyoritsu-Shuppan, Tokyo (in Japanese).

Zolitschka, B., 1998. A 14,000 year sediment yield record from western Germany based on annually laminated lake sediments. Geomorphology 22 (1), 1–17. https://doi.org/10.1016/S0169-555X(97)00051-2.